Modeling Earth Systems and Environment (2025) 11:88
https://doi.org/10.1007/s40808-024-02269-9

ORIGINAL ARTICLE

Improved GODAS reanalysis with MOM5 and impact of altimeter assimilation

Hasibur Rahaman[1] · Samir Pokhrel[2] · Subodh Saha[2] · Raheema Rahman[1,3] · Stephen Penny[4,5] · Eric Hackert[6] · James Carton[7] · T. M. Balakrishna Nair[1] · T. Srinivasa Kumar[1] · M. Ravichandran[8]

Received: 7 October 2024 / Accepted: 19 December 2024

Abstract

The National Centers for Environmental Prediction (NCEP) produces operational reanalysis products based on the Global Ocean Data Assimilation System (GODAS) with the Modular Ocean Model (MOM3/MOM4p0d) as a physical model and 3D-Var as the data assimilation method. The Indian National Center for Ocean Information Services (INCOIS) also produces operational ocean analysis with the same GODAS with MOM4p0d. In this study, GODAS is upgraded with MOM5. The improved reanalysis is compared with respect to the EN4 and Ocean ReAnalysis System 5 (ORAS5) for the subsurface temperature and salinity. The microwave-based satellite-derived sea surface temperature (SST) is employed for the independent evaluation of the reanalysis SST products. We have assimilated observed temperature and salinity profiles from all in situ platforms over the global ocean and also assimilated along-track sea level anomaly from altimeter (Jason1 and Jason2) to produce the improved reanalysis. There is a significant improvement in the SST with biases of temperatures reduced from 1.5 to ~0.2 °C as compared to without assimilation. Moreover, a significant improvement is found in the subsurface temperature and salinity fields over the northwest Atlantic and Pacific Ocean, Nino 3.4, and Indian Ocean thermocline ridge regions. The biases in this new, improved reanalysis are even lower than ORAS5 when compared with EN4 analysis. Thermocline depth also shows improvement in terms of better representation and capturing seasonal variability. Altimeter assimilation further reduces Root Mean Square Deviation (RMSD) in SST over the global ocean. We also show the improvement in the new reanalysis with respect to the reanalysis based on MOM4p0d.

Keywords Ocean reanalysis · Global Ocean Data Assimilation System · Altimeter · Objective analysis

✉ Hasibur Rahaman
rahman@incois.gov.in

Samir Pokhrel
samir@tropmet.res.in

Subodh Saha
subodh@tropmet.res.in

Raheema Rahman
r.rahman-rf@incois.gov.in

Stephen Penny
steve.penny@noaa.gov

Eric Hackert
eric.c.hackert@nasa.gov

James Carton
carton@umd.edu

T. M. Balakrishna Nair
bala@incois.gov.in

T. Srinivasa Kumar
srinivas@incois.gov.in

M. Ravichandran
ravi.moes@gov.in

[1] Indian National Centre for Ocean Information Services (INCOIS), Hyderabad, India

[2] Indian Institute of Tropical Meteorology, Pune, India

[3] Kerala University of Fisheries and Ocean Studies, Kochi, India

[4] Sofar Ocean Technologies, San Francisco, USA

[5] Cooperative Institute for Research in Environmental Sciences, Boulder, USA

[6] Global Modeling and Assimilation Office, NASA, Goddard Space Flight Center, Greenbelt, USA

[7] Department of Atmospheric and Oceanic Science, University of Maryland, College Park, USA

[8] Ministry of Earth Sciences, New Delhi, India

Published online: 20 January 2025

Introduction

Ocean and sea ice analyses and reanalyses are reconstructions of the ocean and sea ice states using an ocean general circulation model integration by atmospheric surface forcing and ocean observations via a data assimilation (DA) method. DA of the global ocean typically suffers from multiple sources of error, including sparse observations, representativeness errors due to the model resolution, poor estimation of background errors, and structural model errors (Storto et al. 2018, 2019). Over the last decade, the performance of ocean analyses and reanalyses has improved mainly due to (a) increased model resolution, (b) improved parameterization of unresolved physics in the models, (c) improved accuracy in forcing from new atmospheric reanalyses (e.g., ERA-I: Dee et al. 2011; JRA55: Tsujino et al. 2018; DRAKKAR: Brodeau et al. 2010), (d) improved quality-controlled observation data sets; and finally (e) advances in DA methods (Storto et al. 2018, 2019).

Ocean reanalyses are a valuable tool for monitoring and understanding long-term ocean variability particularly at deeper ocean (Cipollone et al. 2017), because this part of the ocean is still largely unobserved. Deep and abyssal circulations are crucial for several climate indexes (Masina et al. 2011) that can affect predictability over long time scales. Ocean reanalyses have been used for the initialization of ocean and sea ice components of seasonal to decadal forecasting systems (e.g., at India Meteorological Department (IMD), Met Office, European Centre for Medium-Range Weather Forecasts (ECMWF), National Center for Atmospheric Research (NCAR), Geophysical Fluid Dynamics Laboratory (GFDL), The Euro-Mediterranean Center on Climate Change (CMCC), Meteo France, etc.). The importance of the role of the ocean and sea ice in initialization is indeed widely accepted (Balmaseda 2017; Balmaseda et al. 2009, 2015). Despite the growing community interest, ocean reanalyses, and the ocean component of coupled reforecasts and hindcast, are underutilized compared to the atmospheric component. Efforts are being made, for instance, by Copernicus Climate Change Service (C3S), to release the ocean reanalysis component in a timelier manner. The free access to the error growth of the forecast components has led to a better assessment of forecasting error and bias correction (Storto et al. 2019).

Coupled General Circulation Models (CGCMs) used for the Indian Summer Monsoon Rainfall (ISMR) forecast (Pokhrel et al. 2013; Saha et al. 2014, 2019). Although CGCMs outperform Atmospheric General Circulation Models (AGCMs) in representing the coupled feedback mechanisms of the Earth (Chaudhari et al. 2013, 2015), ISMR prediction skill is still very low despite all the efforts devoted to its improvement (Pokhrel et al. 2016). One of the reasons for the poor performance of these CGCMs in predicting ISMR is the initialization strategy (Saha et al. 2016, 2019). A variation in ISMR prediction skill by National Centers for Environmental Prediction (NCEP) Climate Forecast System version 2 (CFSv2) at different lead months (0–3 months) is found to be linked with the combined effects of initial Eurasian snow cover area and sea surface temperature (SST) over the tropical Indian and Pacific oceans (Saha et al. 2016). Several studies show that the El Niño Southern Oscillation (ENSO) is the strongest predictor on the earth, affecting the weather and climate globally on seasonal, inter-annual, and decadal time scales (Philander 1990). Also, past studies have revealed that the interannual variability of ISMR is linked with the ENSO phenomenon (Sikka 1980; Angell 1981; Rasmusson and Carpenter 1983; Ropelewski and Halpert 1987, 1989; Shukla 1987) and about 50% of droughts in India are associated with ENSO (Kripalani and Kulkarni 1996). Despite ENSO originating and developing in the eastern and central Pacific, it influences the global weather and climate, particularly on the regional scale of precipitation variability in the continents (e.g., Rasmusson and Carpenter1982; Bradley et al. 1987; Ropelewski and Halpert 1987, 1989; Trenberth et al. 1998; Jin et al. 2008; Tang et al. 2018).

Due to its global impact, skillful ENSO prediction well in advance offers policymakers the ability to consider anticipated climate anomalies and define contingency plans due to their adverse effects on society and the economy. Coupled models are now widely used for studying ENSO mechanisms, simulation, and prediction. Various coupled models have been designed and used for ENSO simulation and prediction. These coupled models include simple models (e.g., Hirst 1986), intermediate coupled models (e.g., Zebiak and Cane 1987), hybrid coupled models (e.g., Barnett et al. 1993; Tang and Hsieh 2002), and fully CGCMs (e.g., Jin et al. 2008; Barnston et al. 2012; Luo et al. 2016). Climate Prediction Centre of National Oceanic and Atmospheric Administration (NOAA), NCEP, and the International Research Institute for Climate and Society (IRI) routinely used dynamical and statistical models to make real-time forecasts of ENSO. Currently, around 18 models with different degrees of complexity from different state-of-the-art operational centers across the world are used for skillful seasonal ENSO predictions at six months and longer time scales lead time at IRI (Barnston et al. 2012; Tang et al. 2018).

The large-scale climate variability associated with ENSO is connected to the slow oscillatory phenomena of the coupled atmosphere–ocean system in the Tropics. Rosati et al. (1997), using a coupled model, showed the importance of correctly representing the initial state of the ocean for ENSO prediction. The "memory" (inertia) of this system resides in

the upper ocean (~250 m), which has a much longer timescale than the atmosphere (Rosati et al. 1997). Thus, it is crucial to determine the initial oceanic state as accurately as possible in order to initialize the coupled models mentioned above. This study explores this aspect to produce a realistic reanalysis using GODAS.

Several studies reasonably well predicted the Indian Ocean Dipole (IOD) and its global influence based on CGCMs (Liu et al. 2011, 2017; Yang et al. 2015). Those studies found that the IOD could be predicted one season in advance. However, some operational CGCMs, e.g., NCEP Climate Forecast System version 2 (CFSv2), still lack the skill to be significantly better than persistence in predicting IOD events, as seen in 1982–2009 hindcast results (Zhu et al. 2015). The reason behind this may also be due to inaccurate initial conditions. Doi et al. (2017) demonstrated the importance of improved ocean analyses in the realistic prediction of IOD. Hence, there is evidence that improvements in ocean analyses can improve seasonal ISMR and IOD prediction. The skill of climate system forecasts at the subseasonal to seasonal (S2S) timescales largely depends on the ocean's initial conditions and, in particular, the upper ocean thermal structure. S2S forecasting is now a routine activity in several operational centers around the world, requiring near-real-time knowledge of the ocean state. Hence, we anticipate that any improvement in upper ocean reanalyses may improve the seasonal ISMR prediction since half of the gain in forecast skill is due to improved ocean initialization (Balmaseda et al. 2010).

The Indian National Centre for Ocean Information Services (INCOIS) provides near real-time global ocean analyses based on MOM4p0d (Ravichandran et al. 2013) using the 3D-Var assimilation system GODAS adopted from NCEP. The INCOIS-GODAS analysis provides the initial conditions to the Indian Institute of Tropical Meteorology (IITM) for the initialization of the coupled model CFSv2, which is used for seasonal prediction of the ISMR (Rao et al. 2019). The accuracy of the GODAS 3D-Var analysis depends upon the background error covariance and observation error covariance matrices. The background error covariance can be estimated from model simulations, and consequently, this estimate can be improved by upgrading the model (Stammer et al. 2010). Rahaman et al. (2016, 2018) have shown the impact of upgraded model simulations on the ocean reanalysis/analyses by using the MOM4p1 version (Griffies 2009) with respect to MOM4p0d (Griffies et al. 2004) in NCEP's GODAS. Further, Pokhrel et al. (2024) have shown improved ISMR skills with this improved reanalysis based on MOM4p1. In 2012, a more advanced version, MOM5 was released. Here, we upgrade the physical model used by the GODAS to MOM5. Presently, temperature and salinity profiles from all in-situ observations over the global ocean are assimilated into the operational INCOIS-GODAS. However, schemes to assimilate altimeter-derived along-track sea surface height (SSH) observations had not yet been implemented in the present INCOIS-GODAS operational analysis products (Ravichandran et al. 2013). Hence, apart from upgrading the GODAS with MOM5, we have also implemented the Behringer (2007) assimilation scheme to assimilate the along-track sea surface height observations from Jason 1 and Jason 2.

Traditionally, in a seasonal prediction system, the focus is on the initialization of the subsurface thermal structure in the tropics (Balmaseda 2017). Also, due to its crucial role in global predictability, the initialization of the subsurface thermal structure is key for successful seasonal predictions (McAdam et al. 2022). Hence, here we focus on the thermal structure from the new reanalysis based on the MOM5-GODAS.

This paper is organized as follows. The model configuration, experiments performed, and data used are given in "Model, experiments, and data" section. Results are given in "ASSIM-TS experiment results" section. The impact of altimeter assimilation and improvement in GODAS-MOM5 with respect to GODAS-MOM4p0d is given in "Improvement in MOM5-GODAS with respect to MOM4p0d-GODAS" section. Finally, "Summary and discussion" section provides the summary and discussions.

Model, experiments, and data

Model configuration and experiments

The MOM5 model is configured globally from 80° S to 90° N. The model uses the tripolar grid developed by Murray (1996). The horizontal grid is a staggered Arakawa B grid with geometric height in the vertical. The ocean surface boundary is computed as an explicit free surface. The meridional resolution is 1⁄4° between 10° S and 10° N, then gradually to 1/2° poleward of 30° S and 30° N. Zonal resolution is a uniform 1/2°. There are 40 layers in the vertical, with 27 layers in the upper 400 m, with a maximum bottom depth of approximately 4.5 km. There is 10 m vertical resolution from the surface to the 240 m depth, gradually increasing to about 511 m in the bottom layer. Vertical mixing is achieved using the nonlocal K-profile parameterization of Large et al. (1994) with an additional tidal mixing scheme (Rahaman et al. 2016), and the horizontal mixing of tracers is achieved using the isoneutral method developed by Gent and McWilliams (1990) and Griffies et al. (1998). The horizontal mixing of momentum uses the nonlinear scheme of Smagorinsky (Griffies and Hallberg 2000).

Three experiments were performed for this study. In the first experiment, no assimilation is performed and named without assimilation (hereafter CONTROL); in the second

experiment, all in-situ observed temperature and salinity profiles were assimilated down to 750 m depth, named ASSIM-TS. Because of the lack of spatial coverage of salinity observations during the early few years of the experimental period, particularly in the Indian Ocean, we also assimilated synthetic salinity profiles constructed from temperature profiles and local T-S climatology like that of Huang et al. (2008). The third experiment is the same as ASSIM-TS, but altimeter-derived along-track SSH observations from Jason 1 and Jason 2 are also assimilated. This experiment is named ASSIM-TSH. The observed salinity and temperature profiles from all in-situ platforms used in all experiments were collected from the USGODAE ftp server (http://www.usgodae.org/pub/outgoing/fnmoc/data/ocn/profile).

In all experiments, the NCEP Reanalysis 2 (R2) surface forcing is used (Kanamitsu et al. 2002). The momentum and turbulent heat fluxes are computed with the bulk algorithm formulation of Large and Yeager (2004) by using NCEP R2 near-surface atmospheric fields. SST from ocean model simulation was used for the flux computation. These surface fluxes were further corrected by restoring the model temperature of the first layer (5 m) toward the daily optimal interpolation (OI) OISST analysis version 2 (Reynolds et al. 2007) with a 10-day restoring time scale in all three experiments. The model surface salinity is restored toward the monthly mean sea surface salinity (SSS) climatology based on the WOD1998 (Conkright et al. 1999) with 30 days restoring time. All these experiments were performed from 2003–2010, and 5-day average (pentad) data was used for this study. The details of the experiments performed are given in Table 1.

Altimeter assimilation

The standard GODAS 3D-Var follows the Derber and Rosati (1989) scheme to assimilate salinity and temperature. To assimilate sea surface height (SSH) observations, modifications are made as described by Behringer et al. (1998) and Ji et al. (2000). The modified 3D-Var scheme minimizes a function,

$$I = \tfrac{1}{2}\left\{\mathbf{X}^{\mathbf{T}}B^{-1}\mathbf{X}\right\} + \tfrac{1}{2}\{[H(\mathbf{X}) - \mathbf{d_0}]^{\mathbf{T}}R^{-1}[H(\mathbf{X}) - \mathbf{d_0}] + [H(\mathbf{LX}) - \delta\mathbf{Z_0}]^{\mathbf{T}}R_{\mathbf{SSH}}^{-1}[H(\mathbf{LX}) - \delta\mathbf{Z_0}]\}$$

where the vector **X** represents the correction to the first-guess prognostic tracers (temperature and salinity) computed by the model, **B** is the background error covariance matrix, $\mathbf{d}_0$ represents the difference between the tracer observations and the first-guess, **H** is an interpolation operator

Table 1 Details of experiments performed

Experiment name	Ocean model	Resolution	Forcing field	Assimilation method	Assimilation window	Assimilated data	Restoration data	SST and SSS Restoring time period
CONTROL	MOM5	Zonal-0.5°×0.5° Meridional 0.5°–0.25°	NCEP-R2	3DVAR		No data assimilation	WOA98 SSS (monthly climatology) (Conkright et al. 1999) Daily Reynolds OISST for SST (Reynolds et al. 2007)	30 days (SSS), 10 days (SST)
ASSIM-TS	MOM5	Zonal-0.5°×0.5° Meridional 0.5°–0.25°	NCEP-R2	3DVAR	10 days	Temperature and salinity profiles over the global ocean 65 ^{0}S–^{0}65 N	WOA98 SSS (annual climatology) Daily Reynolds OISST for SST	30 days (SSS), 10 days (SST)
ASSIM-TSH	MOM5	Zonal-0.5°×0.5° Meridional 0.5°–0.25°	NCEP-R2	3DVAR	10 days	Temperature and salinity profiles over the global ocean 65° S–65° N and along-track SSH from Jason-1 and Jason-2	WOA98 SSS (annual climatology) Daily Reynolds OISST for SST	30 days (SSS), 10 days (SST)

that transforms the first-guess tracers i,e model simulated variables from the model grid to the observation locations, **R** is the observation error covariance matrix, **L** is a linear operator that transforms a vertical column of temperature and salinity corrections into an estimate of the correction to the first guess dynamic height field, $\mathbf{R_{SSH}}$ is the observation error covariance matrix for SSH, and $\delta\mathbf{Z_0}$ represents the difference between the observed and first-guess SSH fields. The observational errors are assumed to be uncorrelated, so the matrices R and R_{SSH} have only diagonal elements, which are the error variances of the observations. The last term on the right-hand side is a constraint imposed by the observed SSH. Instead of correcting the model SSH directly, SSH observations are used to impose an integral vertical constraint on the corrected model temperature and salinity fields. The relative magnitudes of these corrections throughout the water column depend on the vertical structure of the first-guess error covariance matrix. In other words, the assimilation system preferentially corrects the model temperature and salinity where their expected errors are greatest, making those corrections in such a way as to bring the model surface dynamic height into closer agreement with the SSH observations. An implied assumption in this approach is that we can use the SSH observations to correct only the baroclinic part of the model SSH and that it is safe to neglect the barotropic part. In the Tropics, our main region of interest, this may be a reasonable assumption (Behringer 2007).

Data used for the evaluation

The SST simulated by all three experiments has been evaluated with microwave-based Advanced Microwave Scanning Radiometer (AMSR-E) observations (Wentz et al. 2014). It is to be noted that daily OISSTv2 Advanced Very High-Resolution Radiometer (AVHRR) only SST data have been used for the surface restoration in the present analysis (Reynolds et al. 2007) for all experiments. Reynolds et al. (2007) suggest that the random error in a revised version of the OISSTv2 analysis is as large as 0.6 °C in the humid tropics, upwelling zones, and marginal ice zones, declining to less than 0.2 °C in the dry subtropics. Hence, AMSR-E SST can be considered an independent dataset for evaluation. We have averaged the daily AMSR-E SST data into concurrent 5-day (pentad) SST analyses. The first model level data at 5 m depth is used as model SST for all the comparisons. The 0.25-degree AMSR-E data have been regridded onto the GODAS grid for all the comparison.

We also use the quality-controlled monthly objective analyses EN4 1° gridded ocean temperature and salinity data to evaluate the subsurface temperature and salinity simulations (Good et al. 2013). In order to see how the present reanalysis performed compared to other reanalysis products, we use the most recent Ocean ReAnalysis System 5 (ORAS5) reanalysis, obtained from http://apdrc.soest.hawaii.edu/datadoc/ecmwf_oras5_1x1.php, which has already been remapped onto a 1° × 1° Mercator horizontal grid (Zuo et al. 2019). The ECMWF OCEAN5 system is a global ocean and sea-ice ensemble of reanalysis and real-time analysis. The OCEAN5 system is a global eddy-permitting ocean-sea ice ensemble (5 members) reanalysis-analysis system. It comprises a Behind-Real-Time (BRT) component that was used for the production of ORAS5 and provides an estimate of the historical ocean state from 1979 to the present (with a few days delay); and a Real-Time (RT) component, that provides the latest ocean conditions for NWP applications. Five (5) ensemble members (opa0-4; with opa0 as the control member without perturbation), were generated using perturbed initial conditions (see Zuo et al. 2019) + observation and forcing perturbations (see Zuo et al. 2015). We also used independent CTD observations taken from specific field campaigns (Rao et al. 2011) over the Bay of Bengal for the evaluation of MOM4p0d-GODAS and MOM5-GODAS. All the data sets used for the evaluation are given in Table 2.

Metrices used for the evaluation and its importance

To evaluate the quality of the reanalysis products we used different metrices. These include the evaluation of SST

Table 2 Data used for the evaluation

Data used	Spatial resolution	Temporal resolution	Type of data	References
EN4	Zonal-1° × 1° Meridional 1° × 1°	Monthly	Temperature and salinity profiles (analysis)	Good et al. (2013)
ORAS5	Zonal-1° × 1° Meridional 1° × 1°	Monthly	Temperature and salinity profiles (reanalysis)	Zuo et al. (2019)
OISSSTv2	Zonal-0.25° × 0.25° Meridional 0.25° × 0.25°	Daily	Sea surface temperature (analysis)	Reynolds et al. (2007)
AMSR-E	Zonal-0.25° × 0.25° Meridional 0.25° × 0.25°	Daily	Sea surface temperature (only satellite from microwave sensor)	Wentz et al. (2014)
CTD	–	Hourly	Temperature and salinity profiles at 89° E, 18° N (North Bay of Bengal)	Rao et al. (2011)

with independent satellite-derived AMSR-E observations. We show spatial bias, mean, and Root Mean Square Deviation (RMSD). For the subsurface we evaluated upper ocean 0–700 m. We used upper ocean 0–700 depth simulations for the evaluation of temperature and salinity since most of the observations before the Argo era were taken from Expendable BathyThermographs (XBTs) till 700 m depth began in the mid to late 1960s. XBTs have provided about 38% of the global temperature observations obtained between 1970 and 2000 for profiles down to a depth of 300 m and a larger portion for profiles to 700 m depth. During the Argo era, ~ 15% of the global temperature profiles are still from XBT deployments (Goni et al. 2019). We show the 0–700 m depth average mean spatial comparison and its bias with respect to widely used EN4 analysis as well as ORAS5 reanalysis. We also show area average temperature and salinity for a few important climatic regions. These are over Nino 3.4 (170° W–120° W; 5° N–5° S), Northwest Pacific (120° E–140° W; 20° N–40° N), North West Atlantic (70° W–50° W; 20° N–45° N) and, Indian Ocean thermocline ridge or dome region (50° E–70° E; 3° S–13° S). As an independent source, we used CTD observation to show the upper ocean temperature and salinity over the BoB. Thermocline depth is another important diagnostic that is used as a metric to evaluate the ocean model simulations. Here, in this study, we evaluated the thermocline depth as a spatial mean and also the time series comparison for a few important climatic regions defined above.

Ocean heat content (OHC) anomalies typically persist for several months, making this variable a vital component of seasonal predictability in both the ocean and the atmosphere (McAdam et al. 2022; Sharma et al. 2022). The thermocline acts as a "memory bank" by providing long-term heat storage over the global ocean, including the tropical Pacific (Neelin et al. 1998). Marine temperature extreme events such as marine heatwaves (MHWs) and marine cold spells (MCSs) are periods of extremes (high and low, respectively) ocean temperatures that persist for days to months (Hobday et al. 2016; Schlegel et al. 2021). MHW impacts the ocean ecology, which includes the shifts in species, impact on the economy through declines in important fishery species, and impacts on aquaculture, which finally affects the seafood industries (Hobday et al. 2016). Recent observational studies show the frequency, intensity, duration, and spatial extent of MHWs have increased substantially in the global ocean (Frölicher et al. 2018; Oliver et al. 2018); on the other hand, MCSs have decreased (Schlegel et al. 2017, 2021) since last few decades. The MCS has become rarer and less severe, while MHW has become more severe, prolonged, and more frequent in the regional seas such as Mediterranean Sea (Simon et al. 2022), Arabian Sea (Chatterjee et al. 2022), Northeast Pacific (de Boisseson et al. 2022), Indian Ocean (Saranya et al. 2022), east and west coast of Australia (Feng et al. 2013; Oliver et al. 2018). Marine heatwaves have approximately doubled in frequency since the 1980s and will continue to increase (Arias et al. 2021), and it is strongest in tropical and Arctic oceans. Saranya et al. (2022) have shown that the western Indian Ocean region experienced the largest increase in MHWs at a rate of 1.2–1.5 events per decade, followed by the north Bay of Bengal at a rate of 0.4–0.5 events per decade during 1982–2018. They also reported that the increased MHWs in the western Indian Ocean and the north Bay of Bengal led to a reduction in monsoon rainfall over the central Indian subcontinent and an enhancement of monsoon rainfall over southwest India due to the MHWs in the Bay of Bengal. Although MHW is mainly defined in terms of SST, a recent study shows the increase in MHW in the last few decades is consistent with oceanic heat content. Reliable heat content from reanalysis products will improve the understanding of the spatio-temporal variability of MHW and its future prediction. Hence, we also evaluated the upper ocean heat content.

ASSIM-TS experiment results

Sea Surface temperature

Seasonal forecasts are sensitive to the initialization of the ocean component of the coupled model, particularly the SST (e.g., Saha et al. 2016). Hence, we focus on how the SST has improved in the new GODAS analysis based on MOM5. Figure 1 shows the spatial distribution of SST bias with respect to AMSR-E SST over the global ocean. It shows a basin-wide warm SST bias of ~ 0.7–0.8 °C in the control run in which no assimilation is performed (Fig. 1a). A few locations in the western boundary currents, such as the Gulf Stream, Kuroshio current, and Agulhas current show a large positive bias of about 1.5 °C (Fig. 1a) in the control experiment. The Southern Ocean, including the Indian, Pacific, and Atlantic Oceans, also shows a slightly higher positive bias (~ 0.5–1 °C) as compared to the topical region. The equatorial region shows an opposite trend with a slight cool SST bias in the CONTROL (no-assimilation) experiment. The warm biases in the CONTROL experiment were reduced to only ~ 0.2–0.3 °C over most of the global ocean in the GODAS ASSIM-TS experiment that assimilates observed temperature and salinity (Fig. 1b). However, the warm bias with reduced amplitude remains over the western boundary current regions and eddy-rich subtropical regions of the southern hemisphere. The SST biases in the Gulf Stream region remain large, which may be associated with the misrepresentation of front positions and overshoot of the northward transport of the Gulf Stream (Zuo et al. 2019) and due to the errors in the NCEP-R2 forcing fields (Xue et al. 2011). This large bias even persists in the most recent reanalysis products ORAS

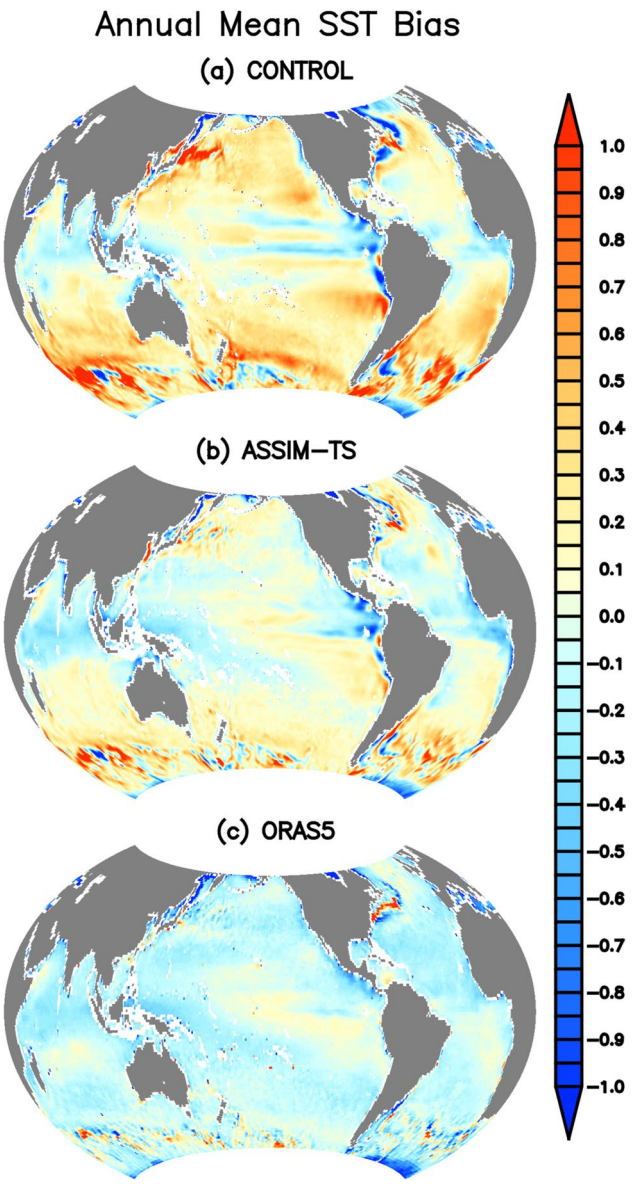

Fig. 1 Mean SST bias (°C) with respect to AMSR-E SST **a** without assimilation (CONTROL), **b** temperature and salinity assimilation in MOM5-GODAS (ASSIM-TS) and **c** ORAS5

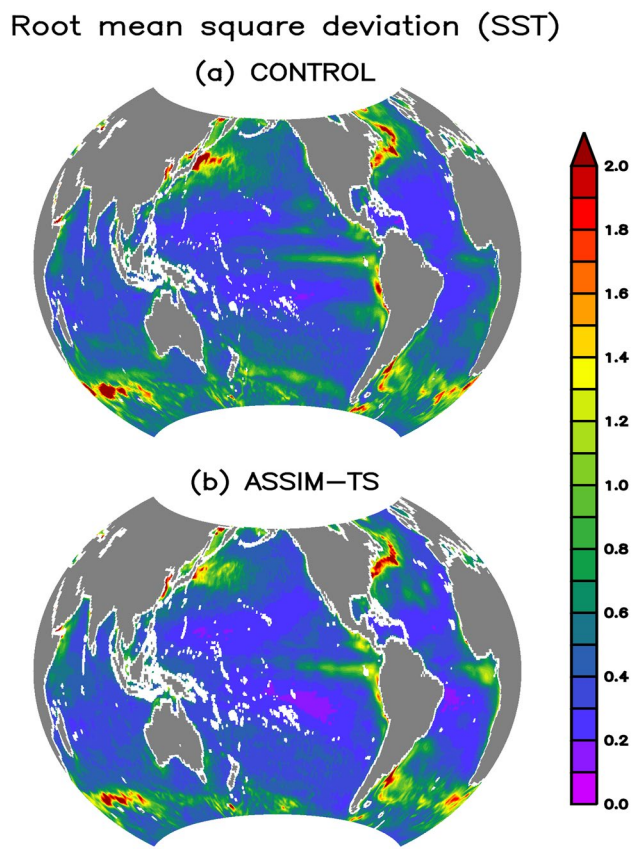

Fig. 2 Root mean square deviation (RMSD) of SST (°C) with respect to AMSR-E observation **a** without assimilation (CONTROL), **b** temperature and salinity assimilation in MOM5-GODAS (ASSIM-TS)

(Fig. 1c). The large cold bias over the Peru upwelling region in the control simulation drastically reduced in the ASSIM-TS experiment. The slightly cold bias over most parts of the Indian Ocean remains almost unchanged in the ASSIM-TS experiment along with the other equatorial basin. It is interesting to note that these cold bias regions also coincide with the warmer SST regions seen in the AMSR-E observations (figure not shown). The ORAS5 SST bias pattern is similar to the ASSIM-TS bias but with reduced magnitude (Fig. 1c). In order to see whether this spatial pattern of bias is stationary in time or it changes with the season, we also show the seasonal bias. The seasonal bias shows a similar pattern, but it shows a seasonal reversal of the bias pattern in winter and summer (figure not shown). In summer, the Northwest and south of 20° S Pacific show a large warm bias (~ 1 °C) in the no assimilation simulation. This pattern reverses in the winter. In seasonal bias, similar improvements can be seen in the ASSIM-TS experiment with the assimilation of temperature and salinity profile (figure not shown).

The amplitude of improvement in the ASSIM-TS experiment can be much visible in the spatial distribution of Root Mean Square Deviations (RMSD) from CONTROL and ASSIM-TS simulations with respect to AMSR-E observations (Fig. 2). The RMSD values over most of the global ocean are between 0.2 and 0.4 °C except few regions, such as western boundary regions. The RMSD values are larger (~ 1–2 °C) in the Gulf Stream and Kuroshio current regions and also in the southern sub-tropical regions in the CONTROL experiment (Fig. 2a). These large RMSD values are reduced significantly with the assimilation of observed temperature and salinity over the global ocean (Fig. 2b). The large RMSD values over the Southern Ocean also reduced significantly. The RMSD values are comparable to CFSR reanalysis RMSD (Xue et al. 2011). The accuracy of SST

variability is also improved in the ASSIM-TS experiment as compared to the CONTROL experiment. The time series of pentad SST RMSD averaged over the global ocean (60° S to 60° S) shows significant improvement in the ASSIM-TS experiment as compared to CONTROL (Fig. 17). See "Impact of Altimeter Assimilation (ASSIM-TSH experiment)" section for further details. In both cases, the RMSD values are high in wintertime (~ 0.5–0.7 °C) in the CONTROL experiment, but these values are reduced to 0.4–0.6 °C in the ASSIM-TS experiment.

Subsurface temp

Since the accuracy of seasonal forecasts largely depends on upper ocean heat content (Balmaseda and Anderson 2009; Balmaseda et al. 2009, 2010, 2015), we expect that the improved upper ocean thermal structure shown in this study may improve seasonal ISMR forecasts. Many previous studies have shown the importance of accurate ocean initialization for the seasonal forecast in coupled ocean–atmosphere general circulation model. Recently, Pokhrel et al. (2024) have shown the impact of improved ocean initialization in the CFSv2 coupled model on ISMR prediction. It is also reported in many previous studies that on a seasonal scale, upper ocean temperature and salinity till 700 m depth influence the seasonal to decadal forecast. Hence, in this study, we have shown upper 700 m temperature and salinity for the evaluation of the MOM5-GODAS reanalysis products. Figure 3 shows the 0–700 m mean temperature from all reanalyses and EN4 analysis. The observed spatial distribution pattern, as represented by ORAS5 and EN4, is mostly captured in the ASSIM-TS experiment, but in the CONTROL experiment, it differs mainly over the northwest Pacific and Indian Oceans. The western basins of all three major oceans, the Pacific, Atlantic, and Indian Ocean, show higher temperatures than their eastern part, except over the equatorial region where the temperature values are similar. This structure resembles the Rossby wave structure and coincides with increased sea level anomalies. The mean 0–700 m

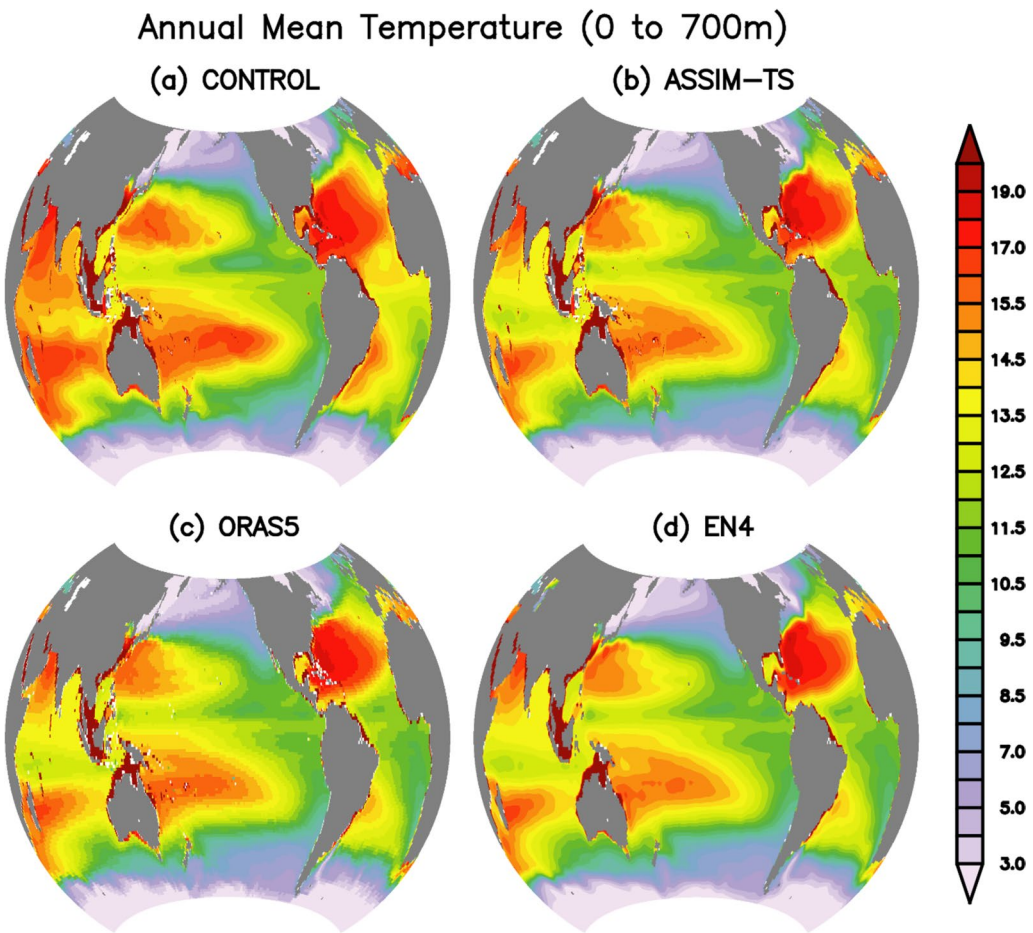

Fig. 3 Upper ocean (0–700 m) annual mean temperature (°C) **a** without assimilation (CONTROL), **b** temperature and salinity assimilation in MOM5-GODAS (ASSIM-TS), **c** ORAS5 and **d** EN4 observation

temperature shows higher values for most of the global ocean, particularly over the Indian Ocean and Northwest Pacific Ocean in CONTROL simulations compared to EN4 analysis (Fig. 3a, d). The upper ocean (0–700 m) temperature structure in the ASSIM-TS experiment is close to the EN4 analysis. This also compares almost similar patterns to ORAS5 (Fig. 3b, c). Because the bias is not quantifiable in Fig. 3, we show the upper ocean (0–700 m) mean temperature bias in CONTROL, ASSIM-TS, and ORAS5 with respect to the EN4 analysis in Fig. 4. The pervasive positive biases in the CONTROL experiment show more than 2 °C in the north Indian Ocean, Northwest Pacific, and the equatorial Atlantic Ocean (Fig. 4a). These large positive biases reduced with T/S assimilation to only ~ ± 0.2 °C

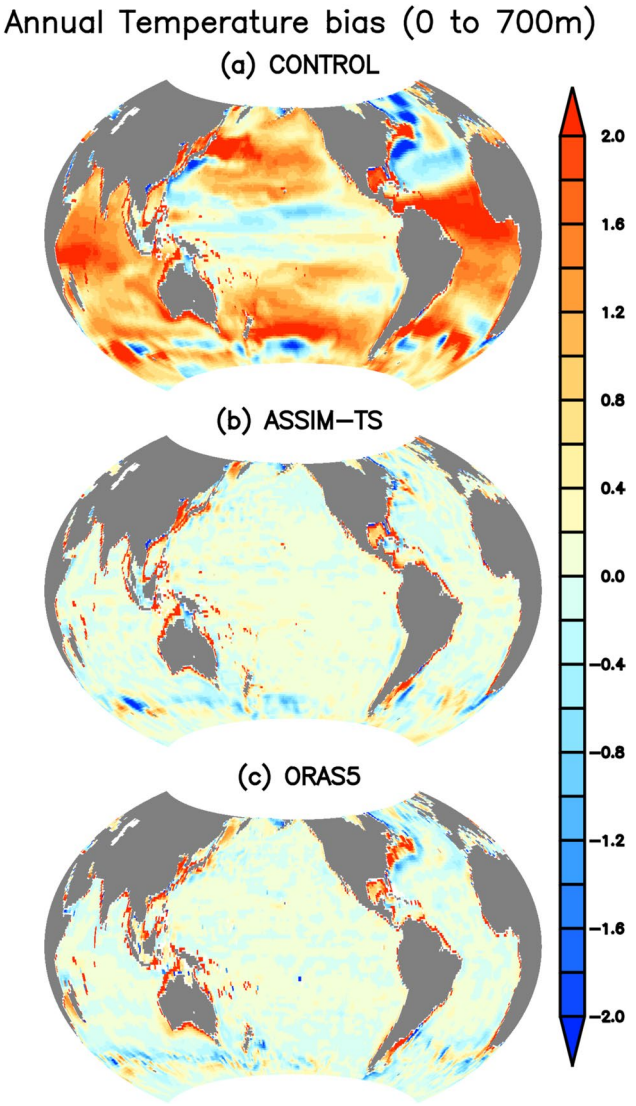

Fig. 4 Upper Ocean (0–700 m) temp bias (°C) with respect to EN4 **a** without assimilation (CONTROL), **b** temperature and salinity assimilation in MOM5-GODAS (ASSIM-TS) and **c** ORAS5

throughout the global ocean except few patches (Fig. 4b). The large negative bias (> 2 °C) in CONTROL over the northwest Atlantic is also reduced in the ASSIM-TS experiment. ASSIM-TS simulation shows much-reduced bias over this region as compared to ORAS5 (Fig. 4b, c). The large positive bias over the Southern Ocean in the CONTROL experiment is also reduced in ASSIM-TS (Fig. 4a, b). A similar result is evident in depth versus longitude plots over the equatorial Indian Ocean and Pacific. The ASSIM-TS experiment shows a reduction in the temperature bias of more than 2 °C over the Indian and Pacific Oceans (figure not shown).

In order to see how the biases vary in the sub-surface in the areas of large positive bias, we show the average temperature profiles over those areas in Fig. 5. Niño 3.4 is a highly studied region in the tropical Pacific Ocean. This important climate region's SST is used to produce El Niño and La Niña indices. Figure 5a shows the upper ocean temperature bias over the Nino 3.4 region from CONTROL, ASSIM-TS, and ORAS5 with respect to EN4. The upper ocean (50–100 m) shows a positive bias ~ 0.5 °C, which is reversed below the thermocline region to a negative bias, and again, it becomes positive below 400 m depth in the CONTROL experiment. On the contrary, the ASSIM-TS experiment shows almost negligible bias except near the thermocline, where there is a slight positive bias (Fig. 5a). However, ORAS5 shows a large positive bias (~ 1 °C) in the thermocline region. Over the Northwest Pacific, the biases reach up to 1.5 °C near the thermocline and remain close to 1 °C throughout the water column in the CONTROL experiment. In the ASSIM-TS experiment, this large positive bias becomes almost zero except for a slight positive bias ~ 0.3 °C below 500 m depth (Fig. 5b). Similar features are also seen over Northwest Atlantic (Fig. 5c). In both these regions, ASSIM-TS bias shows less than ORAS5.

The thermocline ridge region in the southwest Indian Ocean is important due to its influence on the Indian Summer Monsoon and Madden-Julian Oscillation. The presence of an upwelling region in the southwest tropical Indian Ocean (SWTIO) with a shallow thermocline has been named the Seychelles dome or thermocline ridge region. The Seychelles dome or thermocline ridge (TR) has been observed and simulated by many previous studies and attributed to the negative wind stress curl and showed it to be present throughout the year (Xie et al. 2002; Yokoi et al. 2008, 2009; Schott et al. 2009). Several previous studies show that this thermocline dome plays an important role in SST variability across inter-annual, seasonal, and intraseasonal time scales (Xie et al. 2002; Yokoi et al. 2008, 2009; Schott et al. 2009; Vialard et al. 2009). Studies also show ocean wave dynamics efficiently affect SST, allowing SST anomalies to be predicted up to 1–2 years in advance (Qiao et al. 2004, 2016; Fox-Kemper et al. 2019). Hence, we show the

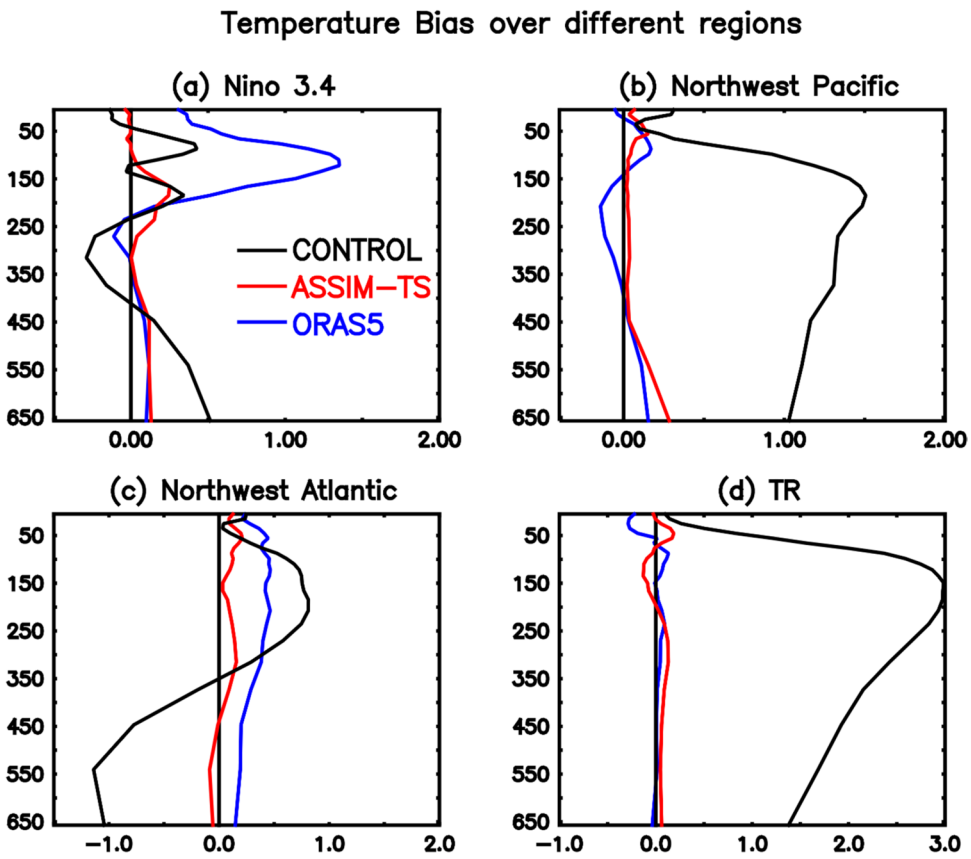

Fig. 5 Upper ocean temperature bias (°C) with respect to EN4 observations over **a** Nino 3.4 (170° W–120° W; 5° N–5° S), **b** northwest Pacific (120° E–140° W; 20° N–40° N), **c** northwest Atlantic (70° W–50° W; 20° N–45° N), **d** Indian Ocean thermocline ridge or dome region (50° E–70° E; 3° S–13° S)

vertical temperature bias over the TR region in Fig. 5d. The subsurface temperature in the CONTROL experiment is too warm in the thermocline regions with a positive bias of 3 °C, which is slightly reduced to 1 °C around 600 m depth (Fig. 5d). However, in the ASSIM-TS experiment, the

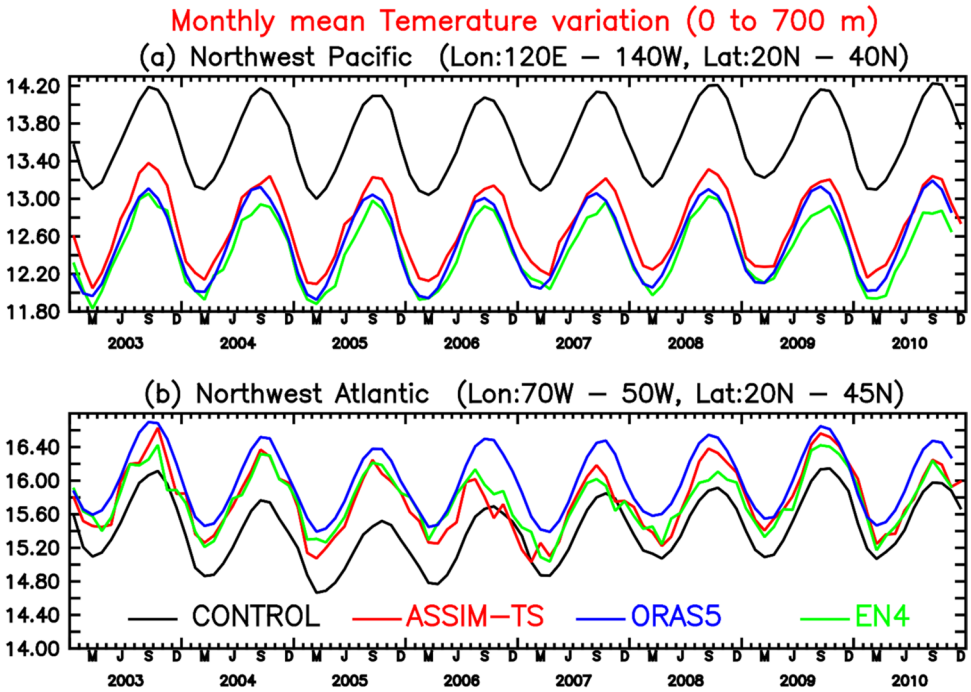

Fig. 6 Inter-annual monthly variation of upper ocean (0–700 m) mean temperature (°C) over **a** northwest Pacific (120° E–140° W; 20° N–40° N), and **b** northwest Atlantic (70° W–50° W; 20° N–45° N)

biases are reduced to near zero when compared with the EN4 analysis.

In order to see whether the significant reduction of 0–700 m average temperature in the ASSIM-TS experiment compared to the CONTROL experiment is sporadic or systematic, we plotted the inter-annual monthly 0–700 m average temperature over the Northwest Pacific and Atlantic in Fig. 6a, b. A prominent annual cycle with a maximum (minimum) peak in September (May) with a mean value of ~ 12.5 °C is seen in the EN4 analysis (green curve). The inter-annual variation of the annual cycle is well captured by both simulations but with a systematic positive bias of ~ 1 °C in the CONTROL experiment (black curve). This systematic bias is reduced to 0.3 °C in the ASSIM-TS experiment (red curve). Considering that the average water column is up to 700 m, this improvement is quite significant. The North Atlantic also shows similar variations but with large inter-annual variability of the annual cycle (Fig. 6b).

Thermocline depth

Despite improvements in model physics and numerics, almost all state-of-the-art ocean general circulation models overestimate the thermocline temperature (e.g. Rahaman et al. 2020). Hence, it is worth examining how the model simulations perform compared to an analysis product that is not dependent on a numerical model i,e., with EN4. Figure 7 shows the depth of the 20 °C isotherm (D20) representing the thermocline depth bias from CONTROL,

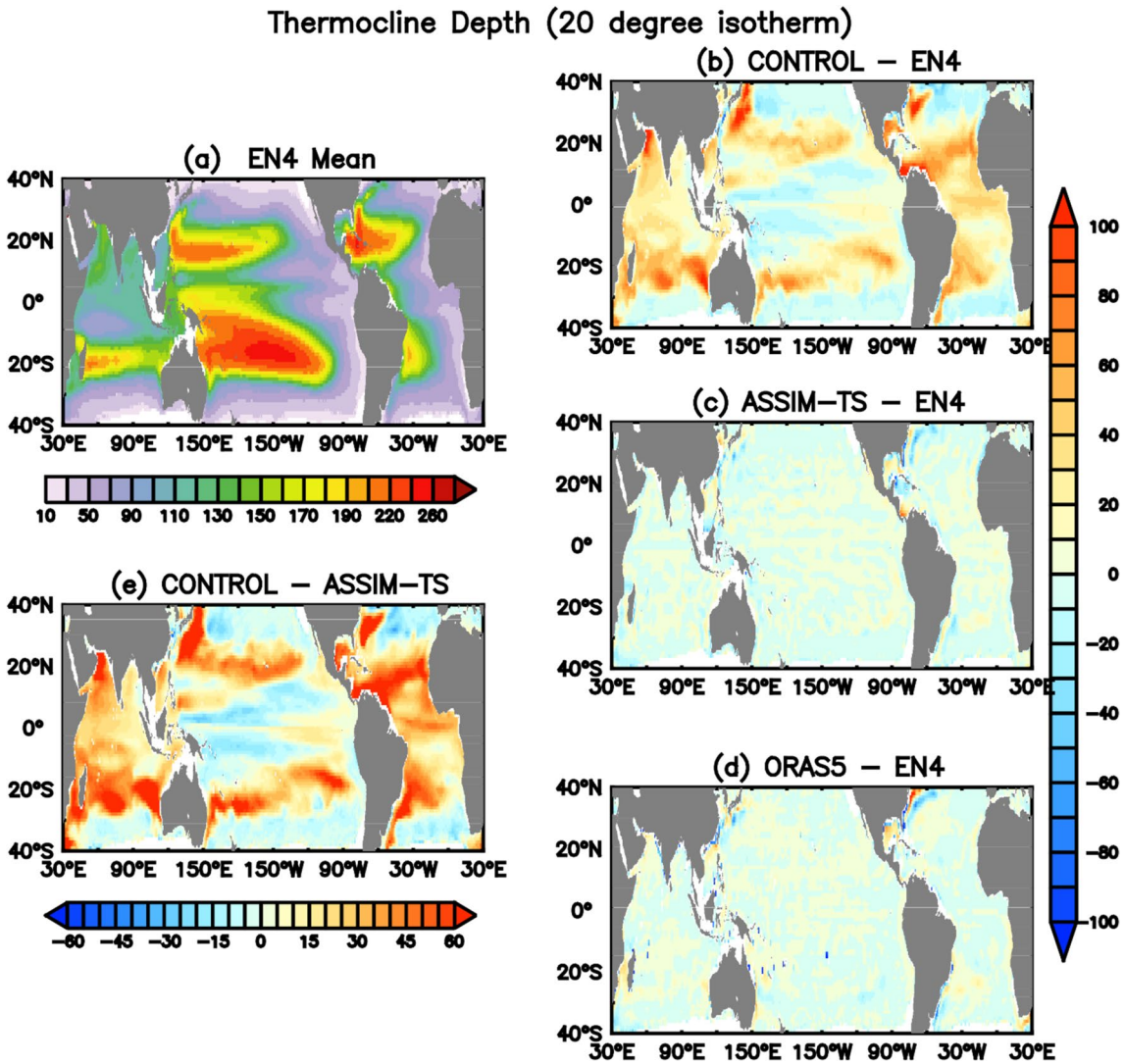

Fig. 7 Spatial distribution of thermocline depth (m) over the global ocean **a** mean D20 from EN4 observation, D20 bias, **b** without assimilation (CONTROL), **c** temperature and salinity assimilation in MOM5-GODAS (ASSIM-TS), **d** ORAS5 and **e** D20 difference between CONTROL and ASSIM-TS

ASSIM-TS, and ORAS5 with respect to the EN4 analysis. The observed mean thermocline is too deep to the east of the subtropical gyre in the Pacific and Atlantic basin and also in the southern Indian Ocean centered along 20° S (Fig. 7a). The CONTROL experiment produces a deeper thermocline (Fig. 7b). An improvement can be seen in the ASSIM-TS experiment, which shows close agreement with the EN4 analysis with biases of only ~ 10 m. Assimilating temperature and salinity corrects the thermocline by more than 60 m in the deeper thermocline regions over the global ocean (Fig. 7c). As explained in "Subsurface temp" section, over SWTIO, a unique open ocean upwelling exists, due to which the thermocline shows shallow over this region compared to other parts of the Indian Ocean. This region shows significant improvements in the ASSIM-TS experiment as compared to the CONTROL experiment (Fig. 7e). The ORAS5 D20 spatial distribution is very close to the EN4 analysis, which the ASSIM-TS experiment also shows (Fig. 7a, c, d). The spatial difference plots show almost identical for ASSIM-TS and ORAS5 (Fig. 7c, d). The difference plots between the CONTROL and ASSIM-TS experiments indicate a much deeper D20 in the CONTROL experiment over the Indian and Atlantic Oceans (Fig. 7e). Over the Pacific Ocean, the D20 in the CONTROL experiment is deeper than most regions except the western equatorial Pacific, where the ASSIM-TS experiment produces a slightly deeper D20 than the CONTROL experiment (Fig. 7e).

In order to examine the inter-annual variability of D20, we show the time series of D20 over the northwest Pacific, northwest Atlantic, southwest Pacific, and Indian Ocean (thermocline dome) region in Fig. 8. Over the Northwest Pacific, a dominant annual cycle with deeper (shallower) D20 is observed during winter (summer). Although the CONTROL experiment captures this observed mode, it is systematically too deep with a mean bias of 22 m (Table 3). In comparison, the ASSIM-TS experiment reproduces the observed annual mode with a mean bias of only 1 m. The monthly standard deviation (STD) is also large in the CONTROL experiment (24 m) as compared to the EN4 analysis (18 m). Both the ASSIM-TS experiment and the ORAS5 reanalysis show almost negligible bias with the least RMSD and STD values close to EN4 (Table 3). The inter-annual variability in D20 is not prominent in all simulations and is almost absent throughout the study period over the northwest Pacific Ocean. The monthly D20 variation over the

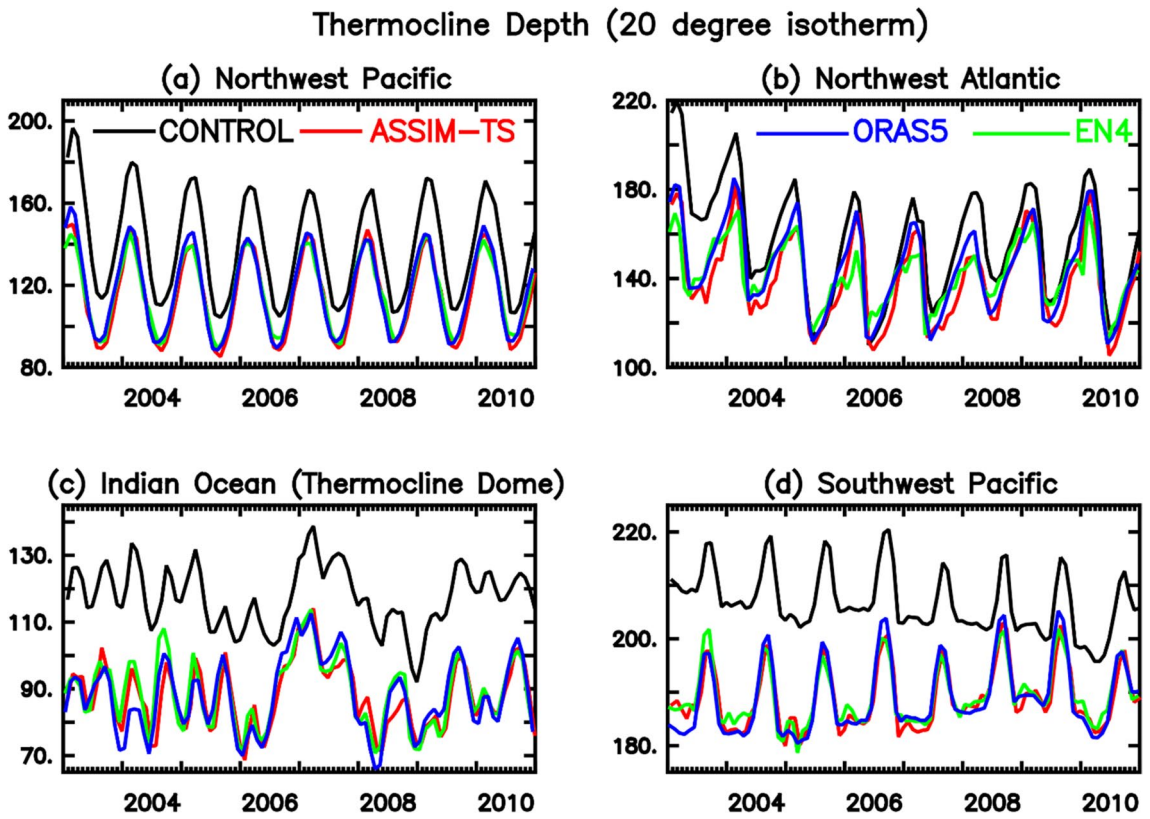

Fig. 8 Inter-annual monthly variation of D20 (m) over **a** northwest Pacific (120° E–140° W; 20° N–40° N), **b** northwest Atlantic (70° W–50° W; 20° N–45° N), **c** Indian Ocean thermocline ridge or dome region (50° E–70° E; 3° S–13° S), and **d** southwest Pacific (150° E–110° W; 10° S–30° S)

Table 3 D20 statists over different regions with respect to the EN4 analysis

	Northwest Pacific			Northwest Atlantic			Indian Ocean Thermocline Ridge			Southwest Pacific		
	Mean (m)	STD (m)	RMSD (m)	Mean (m)	STD (m)	RMSD (m)	Mean (m)	STD (m)	RMSD (m)	Mean (m)	STD (m)	RMSD (m)
EN4	117	18		142	14		89	10		189	5	
CONTROL	139	24	4.5	157	25	5.5	118	9	2.85	207	6	2.4
ASSIM-TS	116	20	1	140	19	1.2	88	10	0.3	189	6	0.06
ORAS5	118	20	1	145	20	1.4	88	11	0.6	189	7	0.35

northwest Atlantic has almost similar seasonality as that of the northwest Pacific, but here, inter-annual variability is prominent. Similar features are observed over the northwest Atlantic Ocean as well. However, over the northwest Atlantic, inter-annual variability is present. Unlike the northwest Pacific, over the northwest Atlantic, the CONTROL experiment shows proximity with the EN4 analysis during the boreal summer months. In the EN4 analysis, mean D20 is deeper over the northwest Atlantic than the northwest Pacific, which was reproduced in both the ASSIM-TS experiment and the ORAS5 reanalysis (Table 3). The RMSD values are only ~ 1 m in both of these regions in ASSIM-TS and ORAS5, while they were as high as ~ 5 m in the CONTROL experiment. The models are able to capture the seasonal variation of D20 over the Seychelles Dome with semiannual cycle peaks during spring and fall (Fig. 8c). However, the CONTROL experiment produces the observed semiannual signal with a constant overestimation, with a mean value of ~ 29 m. The ASSIM-TS experiments accurately capture the observed semiannual signal and the inter-annual variability. We note that this region shows large inter-annual variability as compared to the other two regions mentioned above. The STD values almost replicate the EN4 analysis in both the ASSIM-TS experiment and the ORAS5 reanalysis; also, this region shows RMSD less than 1 m (Table 3). This suggests that data assimilation is effective in reproducing the local Ekman upwelling, resulting from a combination of wind stress curl and the zonal wind stress (Yokoi et al. 2009; Nagura et al. 2013). Due to this unique open ocean upwelling, the mean D20 is only ~ 90 m as compared to 142 m and 117 m over the northwest Atlantic and Pacific Oceans. The inter-annual variability of D20 over the southwest Pacific Ocean from CONTROL, ASSIM-TS, and the EN4 analysis is shown in Fig. 8d. The EN4 analysis shows deeper D20 (~ 200 m) during summer (Aug-Sept), and from November to the following year in May, it shows almost flattened D20 with values of ~ 185 m. The ASSIM-TS experiment and ORAS5 reanalysis almost reproduce this variation with the same mean values of 189 m both in simulations and EN4 analysis (Table 3). The CONTROL experiment reproduced this observed inter-annual variation, but its values are systematically biased deeper by ~ 18 m. The CONTROL and ASSIM-TS experiments also reproduce the inter-annual D20 over the tropical Pacific, but CONTROL shows a large systematic bias of ~ 50 m as compared to ASSIM-TS, which shows only a 20 m bias (figure not shown). The improvements in D20 reconstruction will have a prominent effect on air-sea interaction and may lead to more accurate monsoon forecasts (e.g., Sharma et al. 2022).

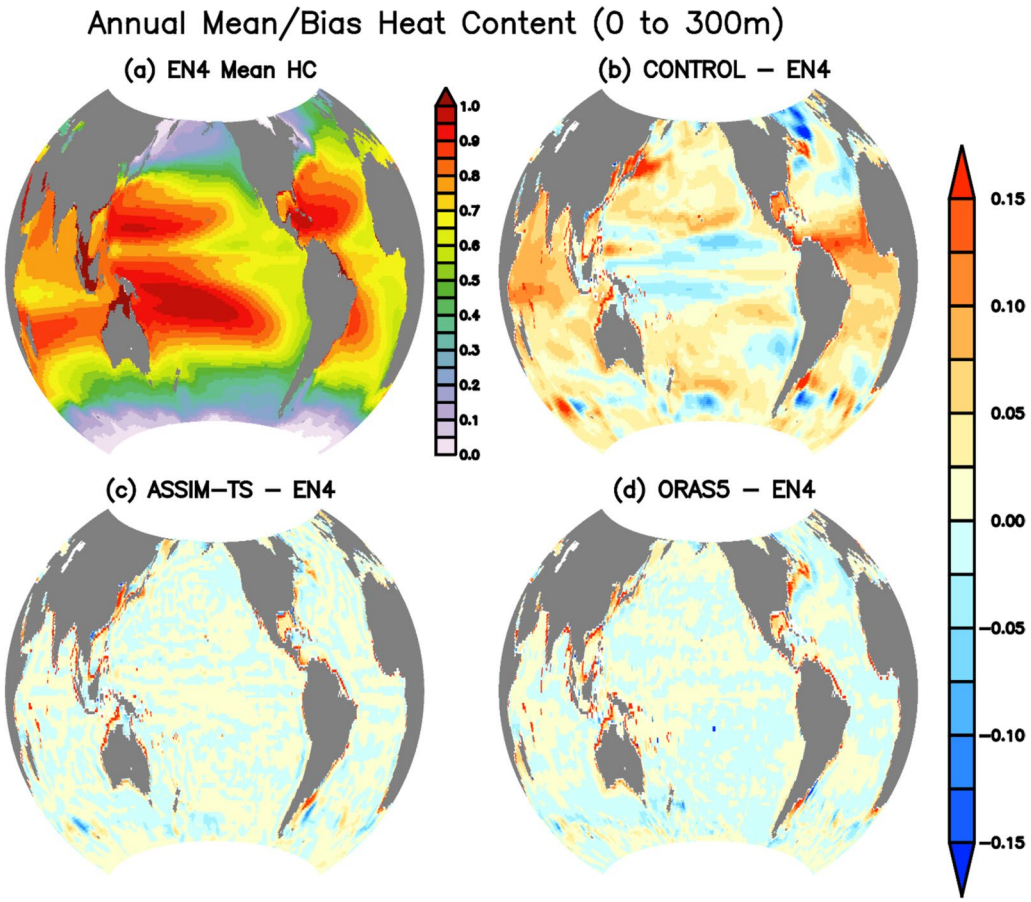

Fig. 9 Upper ocean (0–300 m) annual mean heat content (Joule/m^2) from **a** EN4 analysis and its bias with respect to EN4, **b** without assimilation (CONTROL), **c** temperature and salinity assimilation in MOM5-GODAS (ASSIM-TS) and **d** ORAS5

Upper ocean heat content

This section shows how well the OHC (surface to 300 m depth) from the new MOM5-GODAS reanalysis is reproduced compared to the EN4 analysis and ORAS5 reanalysis products. Estimation of OHC involves temperature and salinity of the ocean; thus, it is a holistic variable that can be used to judge the actual improvement. Figure 9 shows the upper ocean heat content anomaly from CONTROL, ASSIM-TS, and ORAS5. The mean spatial distribution from EN4 is shown in Fig. 9a. Both the mean OHC pattern from the EN4 analysis and its biases from the CONTROL, ASSIM-TS, and ORAS5 follow the pattern of upper ocean temperature bias pattern as evident from the upper ocean bias (see Fig. 4). The impact of temperature and salinity assimilation in the ASSIM-TS experiment from the MOM5-GODAS nearly replicates the bias exhibited by the ORAS5 reanalysis. It is worth mentioning that both the ASSIM-TS and ORAS5 show relatively higher OHC bias near the coast (Fig. 9c, d). The reason could be due to the combination of the inability of the physical model to resolve the coastal process and the lack of observed data, which limits the data assimilation.

Subsurface salinity

The upper ocean salinity variations over the global ocean are the key to estimating thermohaline circulations. Often, models are unable to reproduce the upper ocean salinity variations due to complex air-sea interaction processes and errors in freshwater flux inputs in a forced ocean model. The upper ocean (0–700 m) salinity bias from CONTROL, ASSIM-TS experiments, and the ORAS5 reanalysis with respect to the EN4 analysis are shown in Fig. 10b–d. The mean spatial distribution from the EN4 analysis is also shown in Fig. 10a. The observation shows that the north Atlantic subtropical gyre and the Arabian Sea are the highest salinity regions in the global ocean due to the excess evaporation compared to precipitation (Fig. 10a). High salinity water is also present over the southwest Indian, Pacific, and Atlantic Oceans. On the other hand, low salinity water prevails over the North Pacific, Southern Ocean, and the Indonesian Archipelago

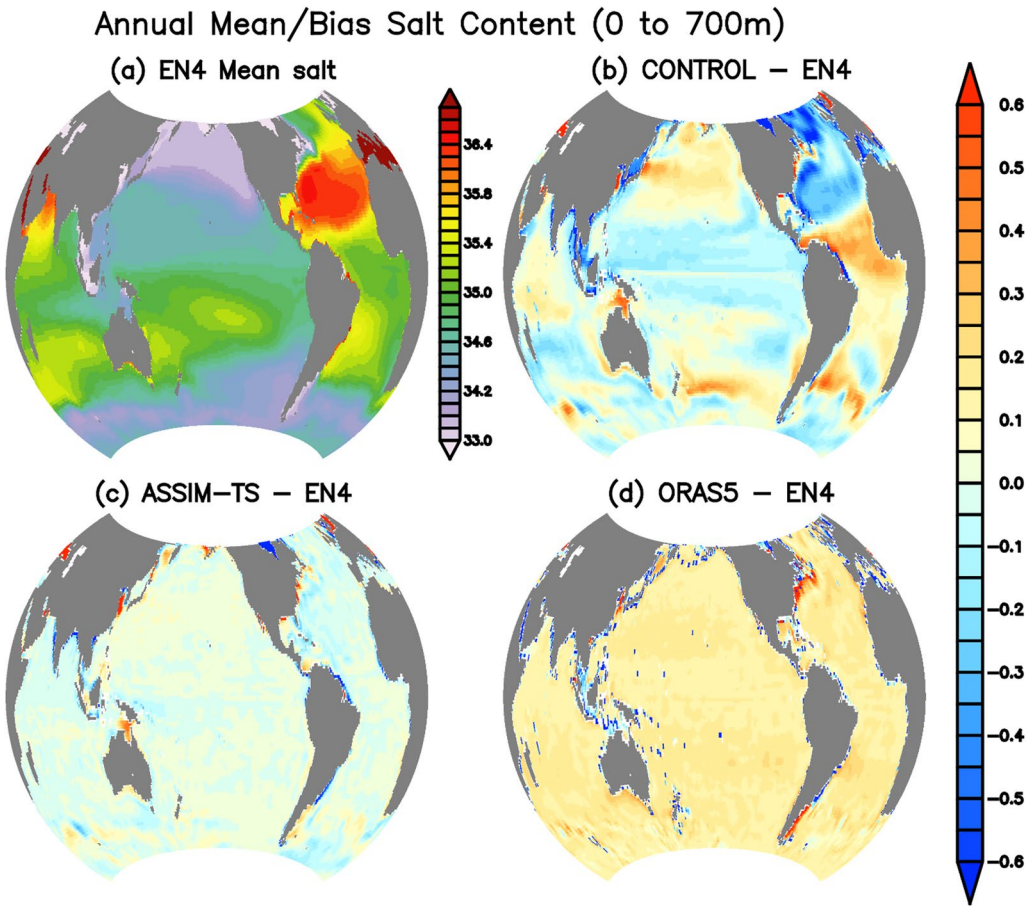

Fig. 10 Upper ocean (0–700 m) annual mean salt (psu) from **a** EN4 analysis, its bias (psu) with respect to EN4, **b** without assimilation (CONTROL), **c** temperature and salinity assimilation in MOM5-GODAS (ASSIM-TS) and **d** ORAS5

regions, including the eastern Bay of Bengal. The CONTROL experiment under (over) estimates high(low) salinity water as compared to observed values (Fig. 10b). The ASSIM-TS experiment almost reproduces the spatial pattern and magnitudes of the EN4 analysis. ASSIM-TS experiment shows biases within the range of ± 0.05 psu almost throughout the global ocean (Fig. 10c). On the contrary, ORAS5 shows a positive bias of ~ 0.05 to 0.15 psu, and these values even reach ~ 0.6 psu over the Gulf Stream region (Fig. 10d). In ASSIM-TS simulation, the biases over the Gulf Stream region are slightly negative (~ 0.1 psu) as compared to EN4 analysis. Overall, minor differences can be seen between the ASSIM-TS experiment and the ORAS5 reanalysis in terms of the distribution pattern.

Most of the previous studies show that salinity variability in the tropical Pacific, particularly in the western Pacific warm pool (WPWP), has been viewed mainly as a passive response to ENSO states and accurately specifying the initial thermal state of the upper tropical ocean is essential for prediction. However, recent observations and modeling experiments suggested that ocean salinity anomaly plays an active role in ENSO evolutions and its forecasts (Zhu et al. 2014; Zhi et al. 2019). In order to see how the upper ocean salinity performs with respect to EN4 analysis, we show the area average salinity difference plots over Nino 3.4 (170° W–120° W; 5° N–5° S), Northwest Pacific (120° E–140° W; 20° N–40° N), North West Atlantic (70° W–50° W; 20° N–45° N) and, Indian Ocean thermocline ridge or dome region (50° E–70° E; 3° S–13° S).

Figure 11 shows the area averaged salinity bias in the upper ocean over the above-stated regions in the global ocean from CONTROL and ASSIM-TS experiments and ORAS5 with respect to the EN4 analysis. The Niño 3.4 region has a negative bias of ~ 0.3 psu at the thermocline depth in the CONTROL experiment, which is reduced in the ASSIM-TS experiment with a negligible value of < 0.1 psu (Fig. 11a). Deeper than the thermocline depth, the salinity bias is almost zero in the ASSIM-TS experiments (Fig. 11a). However, ORAS5 over this important regions shows systematic nearly constant bias ~ 0.15 psu throughout the upper ocean. Hence, initializing with this

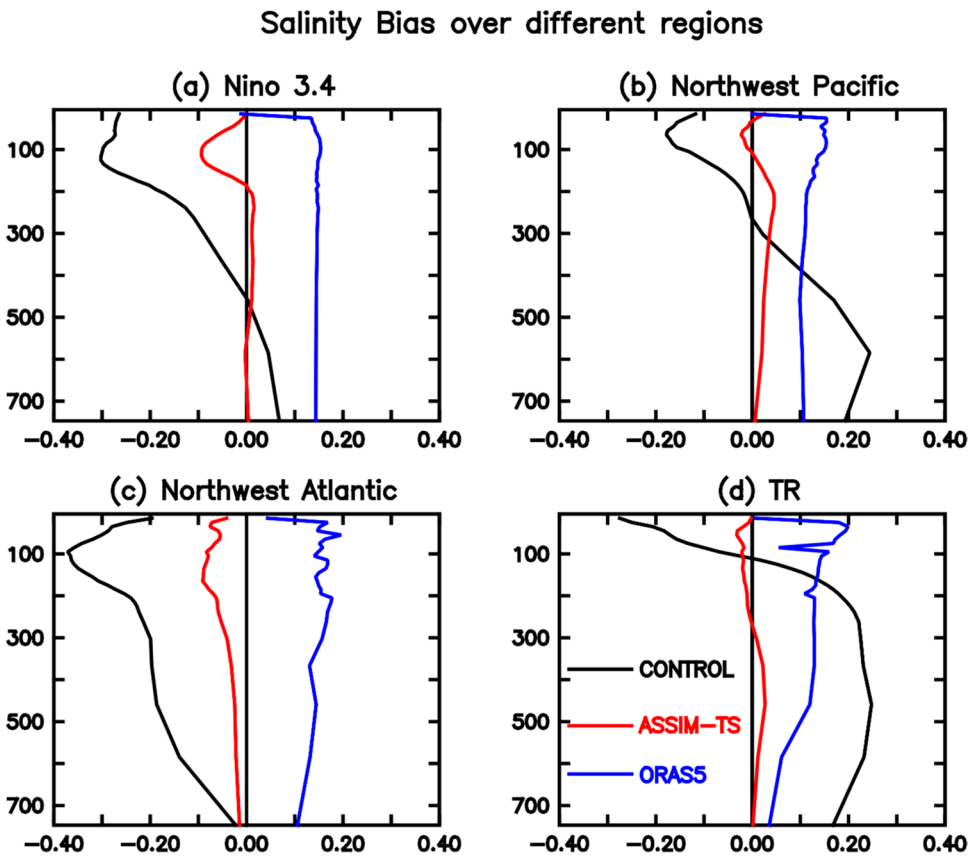

Fig. 11 Upper ocean salt bias (psu) with respect to EN4 analysis over **a** Nino 3.4 (170° W–120° W; 5° N–5° S), **b** northwest Pacific (120° E–140° W; 20° N–40° N), **c** northwest Atlantic (70° W–50° W; 20° N–45° N) and **d** Indian Ocean thermocline ridge or dome region (50° E–70° E; 3° S–13° S)

improved salinity simulation in CGCMs may improve the ENSO and ISMR seasonal forecast. Over the northwest Pacific, the CONTROL experiment has a slight salty bias up to the thermocline depth, which becomes fresher below the 400 m depth. In the ASSIM-TS experiment, the entire upper ocean shows almost negligible bias (Fig. 11b). In this important region, ASSIM-TS simulations outperform with near zero bias compared to ORAS5, which indicates a nearly constant bias of ~ 0.1 psu throughout the upper ocean. Figure 11c shows the salinity bias over the Gulf Stream region i,e over the northwest Atlantic region. This region also shows results similar to those of the Pacific region. The SWTIO has been linked to interannual variability of the ISMR (Thandlam et al. 2023), the Madden–Julian Oscillation (MJO) (Zhu and Kumar 2019), and El Niño Southern Oscillation (ENSO) (Schott et al. 2009; Vialardet al. 2009). The SCTR is a region where the MJO is associated with strong SST variability through strong air-sea interaction feedback (Xie et al. 2002; Yokoi et al. 2008, 2009; Schott et al. 2009; Vialard et al. 2009). The studies show the indirect effect of salinity on MJO variability via its role in upper ocean stratification variability (e.g., the barrier layer), which further modulates intraseasonal SST (Drushka et al. 2012; Guan et al. 2014). Hence, any improvements in upper ocean salinity will directly impact the better prediction of ISMR and MJO. The upper ocean salinity over the TR region almost reproduced the EN4 analysis with near-zero bias throughout the upper ocean (Fig. 11d). Like the Pacific and Atlantic Oceans over the Indian Ocean too, ORAS5 shows a positive salinity bias ~ 0.1–0.2 psu. However, biases are slightly higher in the CONTROL experiment over these regions than in the Niño 3.4 region and northwest Pacific.

Impact of Altimeter Assimilation (ASSIM-TSH experiment)

It has been reported in many previous studies that assimilating SSH observations improves ocean analyses (e.g., Balmaseda and Anderson 2009). Here, we also implement a data assimilation scheme to assimilate along-track altimeter-derived sea surface height (SSH) along with temperature and salinity profiles. The details are given in "Altimeter assimilation" section. In this section, we show the impact of SSH assimilation in MOM5-GODAS.

Figure 12 shows the spatial difference of RMSD computed with respect to AMSR-E SST between ASSIM-TS and ASSIM-TSH over the global ocean. The positive values represent the improvement in SST, and the negative values represent degradation with the SSH assimilation. It can be seen that, except for a few small patches, it shows positive

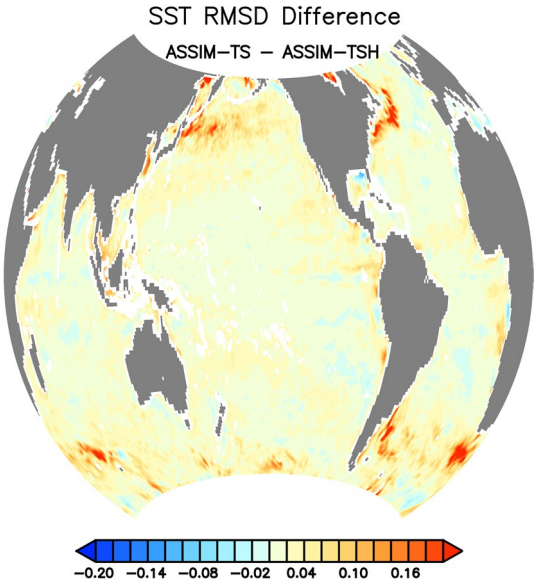

Fig. 12 SST RMSD difference (°C) between ASSIM-TS and ASSIM-TSH experiment over the global ocean

values throughout the global ocean. Significant improvements over the western boundary current regions such as Gulf Stream and Kuroshio Current and over the Northwest Atlantic and Pacific Ocean. The maximum improvement over this region is ~ 0.5 °C. The actual RMSD values over these regions in the ASSIM-TS experiment also show large values of ~ 2 °C. This can be seen in zoom Fig. 13 over the northwest Atlantic. Significant improvements in SST RMSD can be seen along the Gulf Stream path. These improvements can be seen in the subsurface temperature as well over the Gulf Stream region, as shown in Fig. 14. The other regions where the RMSD values are also large are over the southwestern Atlantic region, which is characterized by the poleward flowing Brazil Current (BC) and the equatorward flowing Malvinas Current (MC) and its confluence zone off the coast of Argentina (Combes and Matano 2014) and Southern Ocean also improved (Fig. 15). The improvements in the subsurface temperature off the coast of Argentina in ASSIM-TSH simulations as compared to ASSIM-TS simulations with respect to EN4 analysis can be seen in Fig. 16. Significant improvements are also seen over these regions with the SSH assimilation. These improvements are ~ 20% to 25% over the large RMSD value regions. The large SST bias and RMSD errors at the western boundaries, especially along the Gulf Stream and Kuroshio region, may be related to the misrepresentation of the path of western boundary currents by the model itself (Balmaseda et al. 2015). The previous studies also show that the SST simulation errors over the western boundary current regions are also due to atmospheric forcing errors (Xue et al. 2011).

Figure 17 shows the time series of SST RMSD over the global ocean from ASSIM-TS and ASSIM-TSH experiments with respect to AMSR-E observations. It is worth mentioning that AMSR-E is an independent observation dataset used for SST evaluation. The impact of SSH assimilation can be seen in the reduced RMSD in the ASSIM-TSH experiment compared to the ASSIM-TS experiment. The reduction of RMSD over the global ocean indicates the value added by the assimilation of temperature and salinity, which is further corrected by SSH assimilation in reanalysis products.

The method of Behringer (2007) that we use in assimilating SSH in the GODAS 3Dvar assimilation scheme requires a reference mean climatology of the model corresponding to the mean climatology of the altimeter data used to

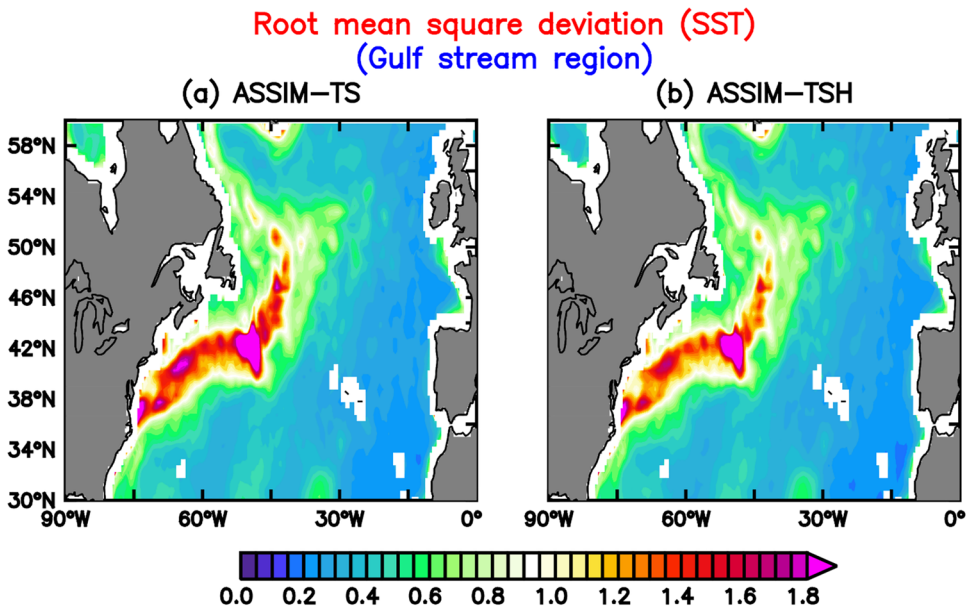

Fig. 13 Spatial distribution of SST RMSD from **a** ASSIM-TS and **b** ASSIM-TSH experiment over North West Atlantic Ocean

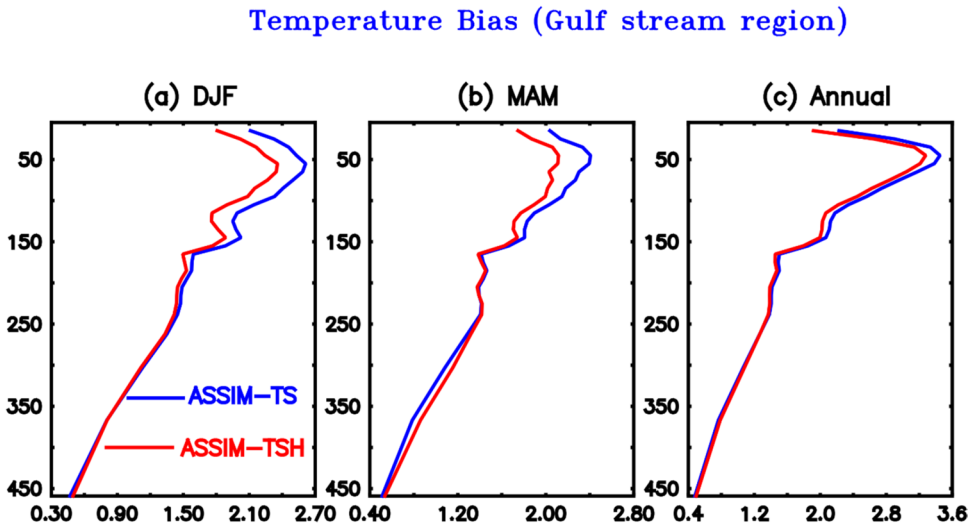

Fig. 14 Upper ocean temperature difference plots averaged over the Gulf Stream region with respect to EN4 analysis from TA and ASSIM-TSH experiments **a** Winter (DJF), **b** Spring (MAM), and **c** annual

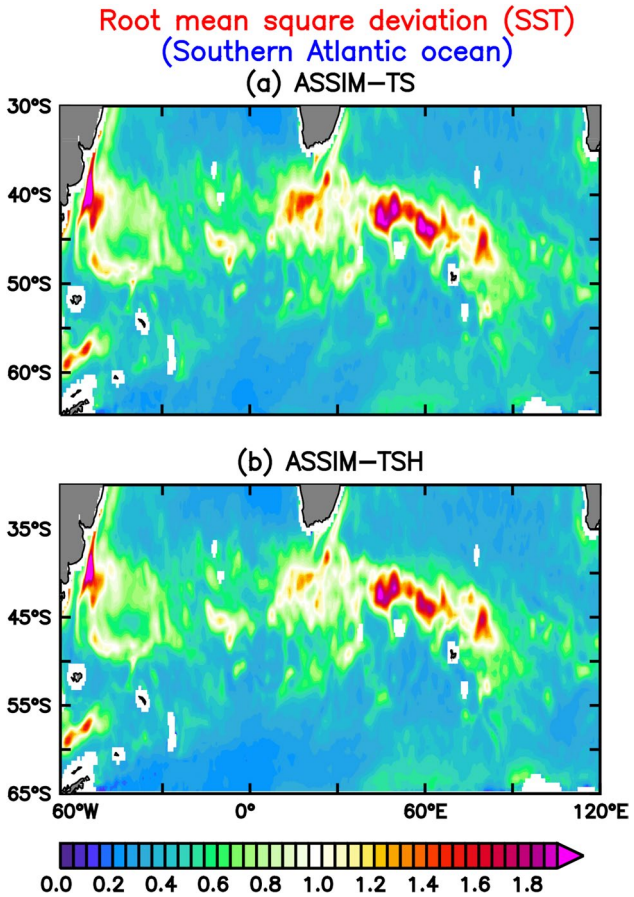

Fig. 15 Spatial distribution of SST RMSD from **a** ASSIM-TS and **b** ASSIM-TSH experiment over the Southern Ocean (south Atlantic sector)

construct the SSH dataset. Computing the model climatology requires a long run of the MOM5-GODAS, assimilating the same in situ data. As this would require considerably greater computing resources, we could not produce such a long reference simulation. Hence, we use the climatology of 2003–2010 for SSH and use this climatology as reference. However, the altimeter data used for the ASSIM-TSH experiment used the 1993–1999 mean as SSH climatology. Due to the different reference periods used for the SSH computation for observation and model, the impact of altimeter assimilation may not show drastic improvement (as reflected in Fig. 12). In this study, we are simply reporting that in the MOM5-GODAS, we also assimilate SSH data derived from altimeters, and it shows improvement. In future studies, we will use the same reference period for computing SSH climatology for observation and model for a longer period of reanalysis.

Improvement in MOM5-GODAS with respect to MOM4p0d-GODAS

In previous studies, Rahaman et al. (2016, 2018) showed improvements in MOM4p1-GODAS as compared to MOMp0d-GODAS. In this section, we briefly show the improvement in subsurface temperature in the MOM5-GODAS as compared to the MOM4p0d-GODAS. Figure 18 shows the upper ocean (0–700 m) mean temperature bias with respect to the EN4 analysis over the global ocean from the MOM5-GODAS and MOM4p0d-GODAS reanalyses. This bias is computed from the 2006–2010 mean. Please note that both of these reanalyses are identical in terms of forcing and data assimilation method (3D-Var and same temperature and salinity profiles) except for the change in the numerical forecast model (MOM4p0d vs MOM5). Overall, the temperature bias was reduced by 0.1 °C using the MOM5-GODAS over most of the global ocean as compared to the MOM4p0d-GODAS. Improvement in the Gulf Stream

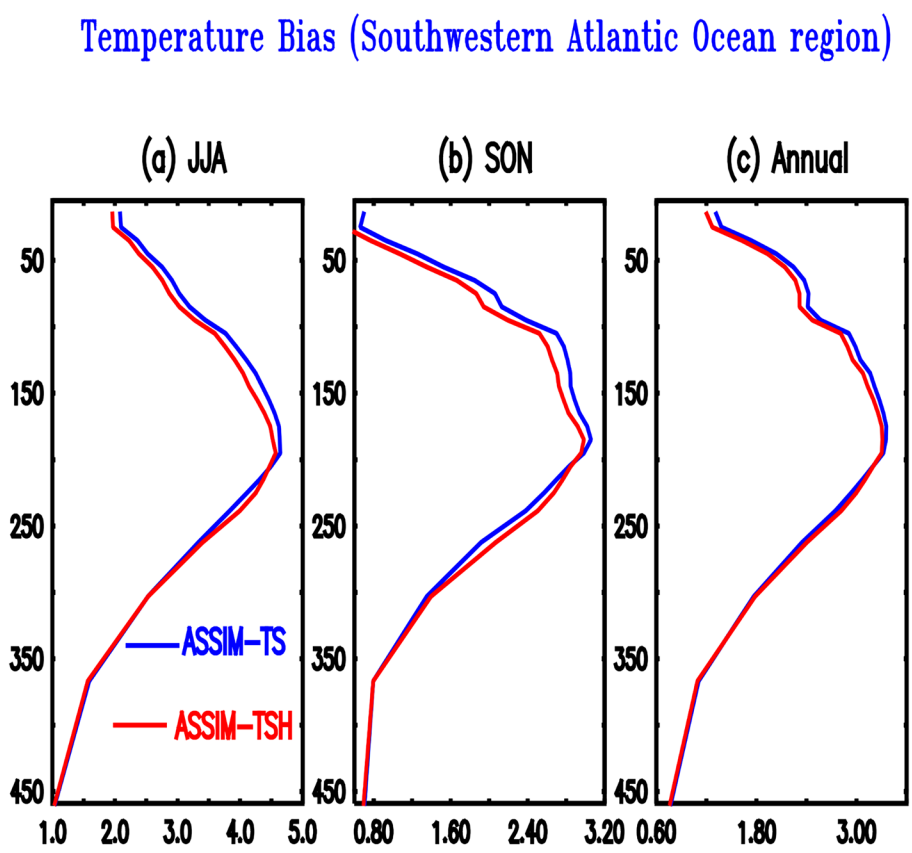

Fig. 16 Temperature difference plots off the coast of Argentina with respect to EN4 analysis from TA and ASSIM-TSH experiments **a** Winter (JJA), **b** Spring (SON), and **c** annual

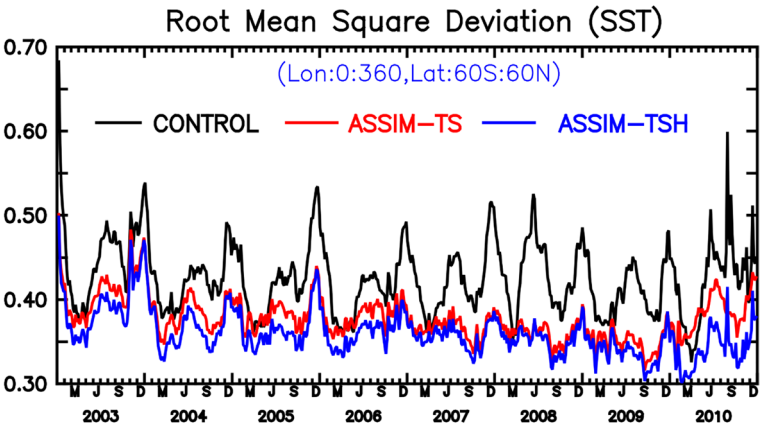

Fig. 17 Inter-annual variation of 5-day SST RMSD (°C) over the global ocean (60° S–60° N)

region in MOM5-GODAS can also be seen as compared to MOM4p0d-GODAS. However, the biases near the coasts still persist and are also slightly enhanced over the Southern Ocean near southern Australia. The interannual variability of ISMR is linked to climate modes such as ENSO, Indian Ocean Dipole (IOD), Atlantic Multidecadal Oscillation (AMO), Atlantic Zonal Mode (AZM), Pacific Decadal Oscillation (PDO) (Hrudaya et al. 2020). The oscillations thought to have the most significant impact on ISMR are ENSO and IOD (Krishnaswami et al. 2015). The IOD has an impact on ISMR, and it also influences the ENSO-ISMR relationship (Ashok et al. 2001; Cherchi et al. 2021). The positive and negative phases of the IOD exhibit asymmetric rainfall variability over India (Behera and Ratnam 2018). Specifically, a positive IOD leads to enhanced ISMR (Ratna et al. 2021).To see how the MOM4p1-GODAS and MOM5-GODAS reanalysis products compare with EN4 over the IOD and ENSO region, we show the depth vs longitude bias of upper ocean temperature over the Indian Ocean and Pacific Ocean along the equator. The improvement in the equatorial Indian Ocean

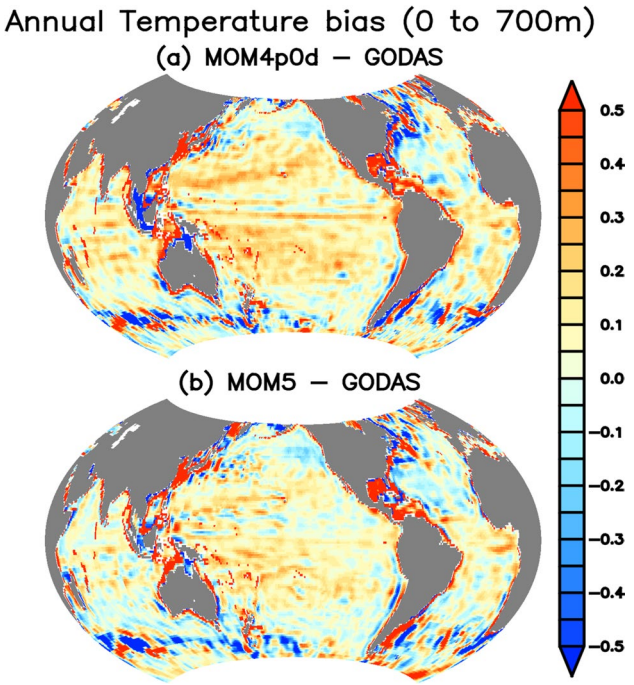

Fig. 18 Upper ocean (0–700 m) temperature bias (°C) with respect to EN4 analysis **a** temperature and salinity assimilation in MOM4p0d-GODAS, **b** temperature and salinity assimilation in MOM5-GODAS (ASSIM-TS)

in MOM5-GODAS as compared to MOM4p0d-GODAS can be seen in Fig. 19. Biases in the western and eastern equatorial Indian Ocean reduced considerably in MOM5-GODAS as compared to operational MOM4p0d-GODAS with respect to EN4 analysis. Similar improvements over the Pacific Ocean can be found in Fig. 20.

One of the challenges in evaluating operational ocean reanalysis is that nearly all high-quality observed temperature and salinity profile data have already been assimilated, making it difficult to validate such reanalysis with independent data. Sometimes, experimental field data can be used to validate such ocean analyses. In our study, we used CTD observations over BoB from July to August 2009 (Rao et al. 2011). Figure 21 shows the mean temperature and salinity comparisons of the new and old GODAS reanalysis during July 2009. Significant improvements in temperature and salinity can be seen in the MOM5-GODAS as compared to the MOM4p0d-GODAS. These improvements can be attributed to the model upgrade since the atmospheric forcing and assimilation schemes are the same.

Summary and discussion

In the last few decades, ocean reanalysis products have been improved significantly due to the improved physical ocean general circulation models and the introduction of sophisticated assimilation schemes such as the Local Ensemble Transform Kalman Filter (LETKF) and the Hybrid-Gain method (Penny 2014; Penny et al. 2015). However, even today, reanalysis products have drawbacks in accurately representing the upper ocean circulation and temperature and salinity structures. The Global Ocean Data Assimilation System (GODAS) is the operational ocean data assimilation system used at NCEP with MOM3 and MOM4 (within the CFS) as the physical OGCM and 3D-Var assimilation scheme (Behringer and Xue 2004; Behringer 2007). The same GODAS system is also operational at INCOIS with MOM4p0d (Ravichandran et al. 2013). Rahaman et al. (2016, 2018), later upgraded the GODAS with MOM4p1 and showed improvements in SST, surface and subsurface currents, upper ocean temperature, and salinity structure over the Indian Ocean. By initializing with this new reanalysis product, the CFSv2 shows improved ISMR prediction skill (Pokhrel et al. 2024). Going further in this study,

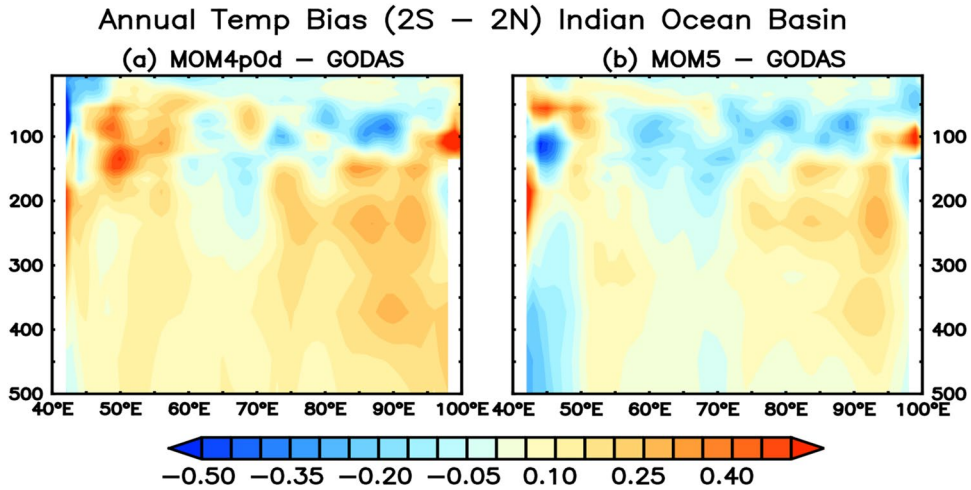

Fig. 19 Depth vs longitude temperature bias (°C) averaged over (2° S-2° N) over the Indian Ocean **a** temperature and salinity assimilation in MOM4p0d-GODAS, **b** temperature and salinity assimilation in MOM5-GODAS (ASSIM-TS)

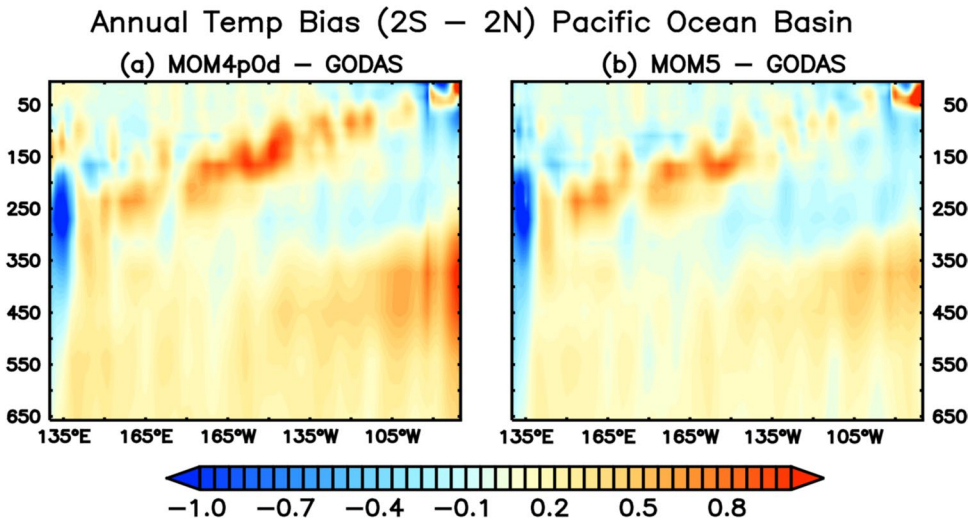

Fig. 20 Depth versus longitude temperature bias (°C) averaged over (2° S–2° N) over the Pacific Ocean **a** temperature and salinity assimilation in MOM4p0d-GODAS, **b** temperature and salinity assimilation in MOM5-GODAS (ASSIM-TS)

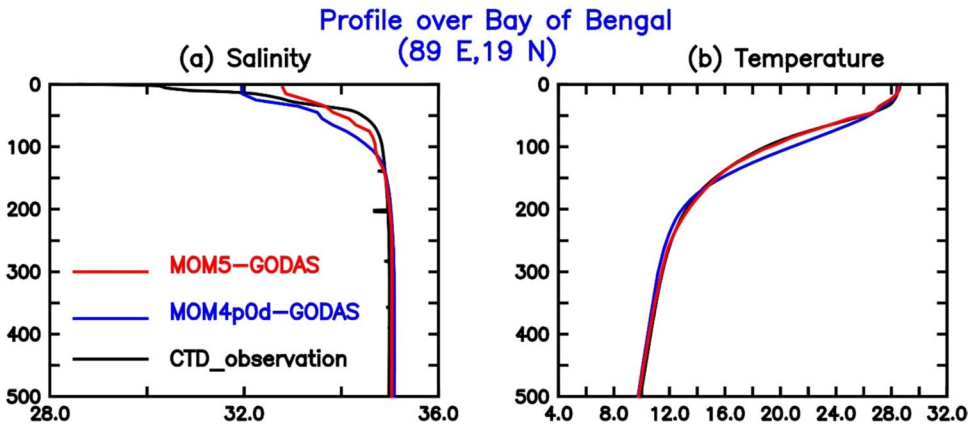

Fig. 21 **a** Salinity (psu), **b** temperature (°C) comparison from MOM5-GODAS and MOM4p0d-GODAS with CTD observation over the north Bay of Bengal during 2009 monsoon (22 July–6 August)

we upgraded the numerical forecast model of the GODAS to MOM5 and implemented the assimilation of altimeter-derived along-track sea surface height (SSH). We assimilated temperature and salinity profile data from all in-situ observing platforms (Argo, Buoy, XBT, etc.) over the global ocean. We performed three experiments: 1. A free run without any data assimilation, named 'without assimilation' (CONTROL), which was used as a control experiment to assess the quality of GODAS; 2. Assimilation of observed temperature and salinity data named ASSIM-TS, and 3. Same as the ASSIM-TS experiment but with additional altimeter along-track SSH data assimilated in GODAS (ASSIM-TSH).

Previous assessments of SST simulation have shown large biases over the northwest Pacific (Taylor et al. 2012; Wang et al. 2014, 2018; Feng et al. 2021), Atlantic Ocean (Taylor et al. 2012; Deppenmeier et al. 2020) and Southern Ocean (Hyder et al. 2018; Wills et al. 2022) in both forced and coupled model simulations. In this study, too, SST bias is larger (~ 1–2 °C) over these regions in simulations without data assimilation (CONTROL). However, in the ASSIM-TS experiment, the biases were reduced drastically and only remained at ~ 0.5 °C, similar to the ORAS5 reanalysis. The SST RMSD values are also large over the regions of large bias in the CONTROL simulation, which was again reduced considerably in the ASSIM-TS experiment. Further assimilation of altimeter derived SSH observations reduced the RMSD over these large RMSD regions. The SSH assimilation preferentially corrects the model temperature and salinity where their expected errors are most significant, making those corrections in such a way as to bring the model surface dynamic height into closer agreement with the SSH observations. Hence, we can expect maximum impact wherever there is a lack of temperature and salinity profiles in the assimilation cycle. Since in the open ocean, the distribution of T/S profiles is reasonably good, we can expect the least impact, whereas near the coastal regions and eddy-rich southern ocean where in-situ temperate and salinity observations are sparse but SSH is available, impacts are more. This is visible with the reduction of SST RMSD over these regions. Producing accurate upper ocean temperature and salinity is crucial for initializing coupled ocean-atmospheric

models for seasonal prediction. Xue et al. (2011) showed that a large spread of reanalysis products from state-of-the-art operational centers is used for the initialization of AOGCMs (Atmosphere–Ocean General Circulation Models), indicating that improving the accuracy and precision of upper ocean temperature and salinity is important for operation prediction. We found that across the experimental configurations that we tested, the most realistic representation of the upper 700 m average temperature was achieved with the MOM5 model when assimilating temperature and salinity observations using the 3D-Var data assimilation technique. The global distribution pattern of 0–700 m average temperature almost replicates the widely used gridded EN4 analysis. On the contrary, the free simulations that do not use any assimilation show a large positive bias (~2 °C) over the northwest Pacific, tropical Atlantic, and the entire Indian Ocean. The distribution patterns of the ASSIM-TS experiment resemble the ORAS5 reanalysis product, which is considered to be a leading ocean reanalysis product (Balmaseda et al. 2015; Zuo et al. 2015, 2019; Karmakar et al. 2018). The ORAS5 reanalysis also uses the 3D-Var data assimilation technique to assimilate SST, SSH, and subsurface temperature and salinity with a 5-day assimilation cycle (Zuo et al. 2019). The thermocline ridge region over the southwest Indian Ocean is unique due to the presence of open ocean upwelling (Xie et al. 2002; Schott et al. 2009; Vialard et al. 2009). This region is the most important for the Indian Summer Monsoon rainfall variability. Many studies show a direct link between ISMR with the SST and upper ocean heat content over this region (Annamalai and Murtugudde 2004; Annamalai et al. 2005; Venugopal et al. 2018). The state-of-the-art OGCMs and IPCC models are unable to simulate the vertical structure of temperature over this region (Rahaman et al. 2020). This is mainly due to the lack of realistic model parameterization schemes, which are mostly independent of model resolution (Rahaman et al. 2020). The present study also shows the thermocline mean temperature is too warm by ~3 °C over this region with no data assimilation. However, with data assimilation, the warm bias almost becomes zero when compared with the EN4 analysis. The inter-annual variability also shows a similar result. The upper ocean mean salinity representation in the ASSIM-TS experiment almost replicates the EN4 observed distribution and also simulations from ORAS5 (a recent study shows ORAS5 is the best product among all reanalysis—Karmakar et al. 2018). We also implemented an assimilation scheme to assimilate along-track altimeter-derived SSH observations. It further shows improvement in the SST and thermocline temperature. This improved upper ocean temperature and salinity structure will provide a more realistic initialization of the CFSv2 coupled model, which is used for the seasonal prediction of ISMR (Saha et al. 2019; Pokhrel et al. 2022).

Acknowledgements The authors thank the ex-director of the Indian National Centre for Ocean Information Services (INCOIS), Dr.S S C Shenoi, for his encouragement in completing this project. The authors thank the data set producer for the free access to these data sets. This is INCOIS contribution no. xxxx. The authors thank David Behringer for providing the 3D-Var assimilation code, including altimeter assimilation. All the plots are made with Data Visualization and Analysis software FERRET, freely available at https://ferret.pmel.noaa.gov/Ferret/

Author contributions H.R. conceived the research plan, generated the new reanalysis products by upgrading GODAS with MOM5, used in this study and prepared the first draft. S.P. performed analysis and generated the figures. H.R. and S.K.S. helped to improve the research plan. All other authors contributed equally for the improvement of the manuscript text.

Funding Funding for this work was provided by Indian National Centre for Ocean Information Services (INCOIS), Ministry of Earth Sciences(MoES), Government of India.

Data availability The reanalysis datasets from GODAS used for this study can be obtained upon request from the corresponding author. All other data sets used in this study such as AMSR-E satellite derived sea surface temperature data and temperature and salinity profiles from ORAS5 reanalysis and EN4 analysis data were obtained from APDRC website (http://apdrc.soest.hawaii.edu/datadoc/ecmwf_oras5_1x1.php), (http://apdrc.soest.hawaii.edu:80/dods/public_data/Reanalysis_Data/Hadley_EN/4.2.1/analyses_g10) and (http://apdrc.soest.hawaii.edu:80/dods/public_data/satellite_product/AMSR/AMSR-E/daily/v7) respectively.

Declarations

Conflict of interest The authors declare no competing interests.

Ethical approval Not applicable.

References

Angell JK (1981) Comparison of variations in atmospheric quantities with sea surface temperature variations in the equatorial Pacific. Mon Weather Rev 109(2):230–243

Annamalai H, Murtugudde R (2004) The role of the Indian Ocean in regional climate variability. Ocean–atmosphere interaction and climate variability. Am Geophys Union Geophys Monogr Ser 147:213–246

Annamalai H, Liu P, Xie SP (2005) Southwest Indian Ocean SST variability: its local effect and remote influence on Asian monsoons. J Clim 18(20):4150–4167

Arias P, Bellouin N, Coppola E, Jones R, Krinner G, Marotzke J et al (2021) Climate change 2021: the physical science basis. Contribution of Working Group14 I to the Sixth Assessment Report of the Intergovernmental Panel on Climate Change; Technical Summary. Cambridge University Press, Cambridge

Ashok K, Guan Z, Yamagata T (2001) Impact of the Indian Ocean dipole on the relationship between the Indian Monsoon Rainfall and ENSO. Geophys Res Lett 28(23):4499–4502. https://doi.org/10.1029/2001GL013294

Balmaseda MA (2017) Data assimilation for initialization of seasonal forecasts. J Mar Res 75(3):331–359

Balmaseda MA, Anderson D (2009) Impact of initialization strategies and observations on seasonal forecast skill. Geophys Res Lett 36(1):L01701. https://doi.org/10.1029/2008GL035561

Balmaseda MA, Aives OJ, Arribas A, Awaji T, Behringer DW, Ferry N et al (2009) Ocean initialization for seasonal forecasts. Oceanography 22(3):154–159

Balmaseda MA, Hernandez F, Storto A, Palmer MD, Alves O, Shi L et al (2015) The ocean reanalysesintercomparison project (ORA-IP). J Oper Oceanogr 8(sup1):s80–s97. https://doi.org/10.1080/1755876X.2015.1022329

Balmaseda M, Fujii Y, Alves O, Lee T, Rienecker M, Rosati T et al (2010) Role of the ocean observing system in an end-to-end seasonal forecasting system. In: Hall J, Harrison DE, Stammer D (eds) Proceedings of OceanObs'09: Sustained Ocean Observations and Information for Society, vol 1, Venice, Italy, 21–25 September 2009. ESA Publication WPP-306. https://doi.org/10.5270/OceanObs09.pp.03

Barnett TP, Graham N, Pazan S, White W, Latif M, Flügel M (1993) ENSO and ENSO-related predictability. Part I: prediction of equatorial Pacific sea surface temperature with a hybrid coupled ocean–atmosphere model. J Clim 6(8):1545–1566

Barnston AG, Tippett MK, L'Heureux ML, Li S, DeWitt DG (2012) Skill of real-time seasonal ENSO model predictions during 2002–11: is our capability increasing? Bull Am Meteorol Soc 93(5):631–651

Behera SK, Ratnam JV (2018) Quasi-asymmetric response of the Indian summer monsoon rainfall to opposite phases of the IOD. Sci Rep 8:123

Behringer DW, Ji M, Leetmaa A (1998) An improved coupled model for ENSO prediction and implications for ocean initialization. Part I: the Ocean Data Assimilation System. Mon Weather Rev 126(4):1013–1021. https://doi.org/10.1175/1520-0493(1998)126%3c1013:AICMFE%3e2.0.CO;2

Behringer DW, Xue Y (2004) Evaluation of the global ocean data assimilation system at NCEP: the Pacific Ocean. Paper presented at the Proc. Eighth Symposium on Integrated Observing and Assimilation System for Atmosphere, Oceans, and Land Surface. American Meteorological Society, Seattle, Washington, 11–15 Jan

Behringer DW (2007) TheGlobalOcean Data Assimilation System at NCEP. Paper presented at 11th Symp. on Integrated Observing and Assimilation Systems for Atmosphere, Oceans, and Land Surface (IOAS-AOLS), San Antonio, TX, Amer. Meteor. Soc., 3.3.Meteor Soc., San Antonio, TX. https://ams.confex.com/ams/87ANNUAL/webprogram/Paper119541.html

de Boisseson E, Balmaseda M, Mayer M, Zuo H (2022) Monitoring and predictions of Marine Heatwave events in the North East Pacific from ocean reanalyses and seasonal forecasts. Paper presented at EGU General Assembly 2022, Vienna, Austria, 23–27 May 2022, EGU22-4079. https://doi.org/10.5194/egusphere-egu22-4079

Bradley RS, Diaz HF, Kiladis GN, Eischeid JK (1987) ENSO signal in continental temperature and precipitation records. Nature 327(6122):497–501

Brodeau L, Barnier B, Treguier AM, Penduff T, Gulev S (2010) An ERA40-based atmospheric forcing for global ocean circulation models. Ocean Model 31(3–4):88–104. https://doi.org/10.1016/j.ocemod.2009.10.005

Chatterjee A, Anil G, Shenoy LR (2022) Marine heatwaves in the Arabian Sea. Ocean Sci 18(3):639–657. https://doi.org/10.5194/os-18-639-2022

Chaudhari HS, Pokhrel S, Mohanty S, Saha SK (2013) Seasonal prediction of Indian summer monsoon in NCEP coupled and uncoupled Model. Theor Appl Climatol 114(3):459–477. https://doi.org/10.1007/s00704-013-0854-8

Chaudhari HS, Pokhrel S, Saha SK, Dhakate A, Hazra A (2015) Improved depiction of Indian summer monsoon in latest high resolution NCEP climate forecast system reanalysis. Int J Climatol 35(10):3102–3119. https://doi.org/10.1002/joc.4196

Cherchi A, Terray P, Ratna SB, Sankar S, Sooraj KP, Behera S (2021) Chapter 8—Indian Ocean Dipole influence on Indian Summer Monsoon and ENSO: a review. In: Indian Summer Monsoon Variability. Elsevier, pp 157–182. https://doi.org/10.1016/B978-0-12-822402-1.00011-9

Cipollone A, Masina S, Storto A, Iovino D (2017) Benchmarking the mesoscale variability in global ocean eddy-permitting numerical systems. Ocean Dyn 67(10):1313–1333. https://doi.org/10.1007/s10236-017-1089-5

Combes V, Matano RP (2014) Trends in the Brazil/Malvinas Confluence region. Geophys Res Lett 41:8971–8977. https://doi.org/10.1002/2014GL062523

Conkright ME, Levitus S, O'Brien TD, Boyer TP, Stephens C, Johnson DR et al (1999) World Ocean Database 1998: CD-ROM data set documentation. Internal report (National Oceanographic Data Center), 14. https://repository.library.noaa.gov/view/noaa/1173

Dee DP, Uppala SM, Simmons AJ, Berrisford P, Poli P, Kobayashi S et al (2011) The ERA-Interim reanalysis: configuration and performance of the data assimilation system. Q J R Meteorol Soc 137(656):553–597. https://doi.org/10.1002/qj.828

Deppenmeier A, Haarsma RJ, van Heerwaarden C, Hazeleger W (2020) The Southeastern Tropical Atlantic SST bias investigated with a coupled atmosphere-ocean single-column model at a PIRATA Mooring Site. J Clim 33(14):6255–6271. https://doi.org/10.1175/JCLI-D-19-0608.1

Derber J, Rosati A (1989) A global oceanic data assimilation system. J Phys Oceanogr 19(9):1333–1347. https://doi.org/10.1175/1520-0485(1989)019%3c1333:AGODAS%3e2.0.CO;2

Doi T, Storto A, Behera SK, Navarra A, Yamagata T (2017) Improved Prediction of the Indian Ocean Dipole Mode by Use of Subsurface Ocean Observations. Journal of Climate 30(19):7953–7970. https://doi.org/10.1175/JCLI-D-16-0915.1

Drushka K, Sprintall J, Gille S, Wijffels S (2012) In situ observations of Madden–Julian oscillation mixed layer dynamics in the Indian and western Pacific Oceans. J Clim 25:2306–2328. https://doi.org/10.1175/JCLI-D-11-00203.1

Feng M, McPhaden MJ, Xie SP, Hafner J (2013) La Niña forces unprecedented Leeuwin Current warming in 2011. Sci Rep 3(1):1–9. https://doi.org/10.1038/srep01277

Feng J, Lian T, Chen D, Li Y (2021) The cause of the large cold bias in the Northwestern Pacific Ocean. Geophys Res Lett 48(18):e2021GL094616. https://doi.org/10.1029/2021GL094616

Fox-Kemper B, Adcroft A, Böning CW, Chassignet EP, Curchitser E, Danabasoglu G et al (2019) Challenges and prospects in ocean circulation models. Front Mar Sci 6:65. https://doi.org/10.3389/fmars.2019.00065

Frölicher TL, Fischer EM, Gruber N (2018) Marine heatwaves under global warming. Nature 560(7718):360–364

Gent PR, McWilliams JC (1990) Isopycnal mixing in ocean circulation models. J Phys Oceanogr 20(1):150–155. https://doi.org/10.1175/1520-0485(1990)020%3c0150:IMIOCM%3e2.0.CO;2

Goni GJ, Sprintall J, Bringas F, Cheng L, Cirano M, Dong S, Domingues R, Goes M, Lopez H, Morrow R, Rivero U, Rossby T, Todd RE, Trinanes J, Zilberman N, Baringer M, Boyer T, Cowley R, Domingues CM, Hutchinson K, Kramp M, Mata MM, Reseghetti F, Sun C, Bhaskar U, Volkov D (2019) More than 50 years of successful continuous temperature section measurements by the Global Expendable Bathythermograph Network, its integrability, societal benefits, and future. Front Mar Sci 6:452. https://doi.org/10.3389/fmars.2019.00452

Good SA, Martin MJ, Rayner NA (2013) EN4: quality controlled ocean temperature and salinity profiles and monthly objective analyses with uncertainty estimates. J Geophys Res Oceans 118(12):6704–6716. https://doi.org/10.1002/2013JC009067

Griffies SM, Hallberg RW (2000) Biharmonic friction with a Smagorinsky-like viscosity for use in largescale eddy-permitting ocean models. Mon Weather Rev 128(8):2935–2946. https://doi.org/10.1175/1520-0493(2000)128%3c2935:BFWASL%3e2.0.CO;2

Griffies SM, Gnanadesikan A, Pacanowski RC, Larichev VD, Dukowicz JK, Smith RD (1998) Isoneutral diffusion in a z-coordinate ocean model. J Phys Oceanogr 28(5):805–830. https://doi.org/10.1175/1520-0485(1998)028%3c0805:IDIAZC%3e2.0.CO;2

Griffies SM, Harrison MJ, Pacanowski RC, Rosati A (2004) Technical guide to MOM4.GFDL Ocean Group (Technical Report No. 5, 342p.). NOAA/Geophysical Fluid Dynamics Laboratory. www.gfdl.noaa.gov/~fms

Griffies SM (2009) Elements of MOM4P1 GFDL Ocean Group (Technical Report 6, 444p.). NOAA/Geophysical Fluid Dynamics Laboratory

Guan B, Lee T, Halkides DJ, Waliser DE (2014) Aquarius surface salinity and the Madden–Julian oscillation: the role of salinity in surface layer density and potential energy. Geophys Res Lett 41:2858–2869. https://doi.org/10.1002/2014GL059704

Hirst AC (1986) Unstable and damped equatorial modes in simple coupled ocean–atmosphere models. J Atmos Sci 43(6):606–632. https://doi.org/10.1175/1520-0469(1986)043%3c0606:UADEMI%3e2.0.CO;2

Hobday AJ, Alexander LV, Perkins SE, Smale DA, Straub SC et al (2016) A hierarchical approach to defining marine heatwaves. Prog Oceanogr 141:227–238. https://doi.org/10.1016/j.pocean.2015.12.014

Huang B, Xue Y, Behringer DW (2008) Impacts of Argo salinity in NCEP Global Ocean Data Assimilation System: the tropical Indian Ocean. J Geophys Res 113:C08002. https://doi.org/10.1029/2007JC004388

Hyder P, Edwards JM, Allan RP, Hewitt HT, Bracegirdle TJ, Gregory JM et al (2018) Critical Southern Ocean climate model biases traced to atmospheric model cloud errors. Nat Commun 9(1):3625. https://doi.org/10.1038/s41467-018-05634-2

Ji M, Reynolds RW, Behringer DW (2000) Use of TOPEX/Poseidon sea level data for ocean analyses and ENSO prediction: Some early results. J Clim 13(1):216–231. https://doi.org/10.1175/1520-0442(2000)013%3c0216:UOTPSL%3e2.0.CO;2

Jin EK, Kinter JL, Wang B, Park CK, Kang IS, Kirtman BP et al (2008) Current status of ENSO prediction skill in coupled ocean–atmosphere models. Clim Dyn 31(6):647–664. https://doi.org/10.1007/s00382-008-0397-3

Kanamitsu M, Ebisuzaki W, Woollen J, Yang SK, Hnilo JJ, Fiorino M, Potter GL (2002) NCEP–DOE AMIP-II Reanalysis (R-2). Bull Am Meteorol Soc 83(11):1631–1644. https://doi.org/10.1175/BAMS-83-11-1631

Karmakar A, Parekh A, Chowdary JS, Gnanaseelan C (2018) Inter comparison of Tropical Indian Ocean features in different ocean reanalysis products. Clim Dyn 51(1):119–141. https://doi.org/10.1007/s00382-017-3910-8

Kripalani RH, Kulkarni A (1996) Assessing the impacts of El Nino and non-El Nino related droughts over India. Dorught Netw News 8:11–13

Krishnaswami J, Vaidyanathan S, Rajagopalan B, Bonnel M, Sankaran M, Bhalla RS, Badiger S (2015) Non-stationary and non-linear influence of ENSO and Indian Ocean Dipole on Indian summer monsoon rainfall and extreme rain events. Clim Dyn 45:175–184. https://doi.org/10.1007/s00382-014-2288-0

Large WG, McWilliams JC, Doney SC (1994) Oceanic vertical mixing: a review and a model with a nonlocal boundary layer parameterization. Rev Geophys 32(4):363–403. https://doi.org/10.1029/94RG01872

Large WG, Yeager SG (2004) Diurnal to decadal global forcing for ocean and sea-ice models: the data sets and flux climatologies. NCAR Technical Note TN-460, 105 pp

Liu L, Yu W, Li T (2011) Dynamic and thermodynamic air–sea coupling associated with the Indian Ocean Dipole diagnosed from 23 WCRP CMIP3 models. J Clim 24(18):4941–4958. https://doi.org/10.1175/2011JCLI4041.1

Liu H, Tang Y, Chen D, Lian T (2017) Predictability of the Indian Ocean Dipole in the coupled models. Clim Dyn 48(5):2005–2024. https://doi.org/10.1007/s00382-016-3187-3

Luo JJ, Lee JY, Yuan CX, Sasaki W, Masso S, Behera SK et al (2016) Current status of intraseasonal–seasonal-to-interannual prediction of the Indo-Pacific climate. In: Behera SK, Yamagata T (eds) Indo-Pacific climate variability and predictability. World Scientific, pp 63–107. https://doi.org/10.1142/9789814696623_0003

Masina S, Di Pietro P, Storto A, Navarra A (2011) Global ocean reanalyses for climate applications. Dyn Atmos Oceans 52(1–2):341–366. https://doi.org/10.1016/j.dynatmoce.2011.03.006

McAdam R, Masina S, Balmaseda M, Gualdi S, Senan R, Mayer M (2022) Seasonal forecast skill of upper-ocean heat content in coupled high-resolution systems. Clim Dyn 58(11):3335–3350. https://doi.org/10.1007/s00382-021-06101-3

Murray RJ (1996) Explicit generation of orthogonal grids for ocean models. J Comput Phys 126(2):251–273. https://doi.org/10.1006/jcph.1996.0136

Nagura M, Sasaki W, Tozuka T, Luo JJ, Behera SK, Yamagata T (2013) Longitudinal biases in the Seychelles Dome simulated by 35 ocean–atmosphere coupled general circulation models. J Geophys Res Oceans 118(2):831–846. https://doi.org/10.1029/2012JC008352

Neelin JD, Battisti DS, Hirst AC, Jin FF, Wakata Y, Yamagata T, Zebiak SE (1998) ENSO theory. J Geophys Res 103(C7):14261–14290. https://doi.org/10.1029/97JC03424

Oliver EC, Lago V, Hobday AJ, Holbrook NJ, Ling SD, Mundy CN (2018) Marine heatwaves off eastern Tasmania: trends, interannual variability, and predictability. Prog Oceanogr 161:116–130. https://doi.org/10.1016/j.pocean.2018.02.007

Penny SG (2014) The hybrid local ensemble transform Kalman filter. Mon Weather Rev 142(6):2139–2149

Penny SG, Behringer DW, Carton JA, Kalnay E (2015) A Hybrid Global Ocean Data Assimilation System at NCEP. Mon Weather Rev 143(11):4660–4677

Philander SG (1990) El Nino, La Nina, and the Southern oscillation. Academic Press, San Diego, p 293

Pokhrel S, Dhakate A, Chaudhari HS, Saha SK (2013) Status of NCEP CFS vis-a-vis IPCC AR4 models for the simulation of Indian summer monsoon. Theor Appl Climatol 111(1):65–78. https://doi.org/10.1007/s00704-012-0652-8

Pokhrel S, Saha SK, Dhakate A, Rahman H, Chaudhari HS, Salunke K et al (2016) Seasonal prediction of Indian summer monsoon rainfall in NCEP CFSv2: forecast and predictability error. Clim Dyn 46(7):2305–2326. https://doi.org/10.1007/s00382-015-2703-1

Pokhrel S, Rahaman H, Saha SK, Chaudhari H, Hazra A, Ravichandran M (2024) Role of improved ocean initial state in the seasonal prediction of Indian Summer Monsoon: a case study. Ocean-Land-Atmos Res 3:0034. https://doi.org/10.34133/olar.0034

Pokhrel S, Rahaman H, Saha SK, Chaudhari H, Hazra A, Ravichandran M (2022) Impact of improved ocean initial condition on the seasonal prediction of Indian Summer Monsoon. Clim Dyn **(Under Review)**

Qiao F, Yuan Y, Yang Y, Zheng Q, Xia C, Ma J (2004) Wave-induced mixing in the upper ocean: distribution and application to a global ocean circulation model. Geophys Res Lett 31(11):L11303. https://doi.org/10.1029/2004GL019824

Qiao F, Yuan Y, Deng J, Dai D, Song Z (2016) Wave–turbulence interaction-induced vertical mixing and its effects in ocean and climate models. Philos Trans R Soc A Math Phys Eng Sci 374(2065):20150201. https://doi.org/10.1098/rsta.2015.0201

Rahaman H, Behringer DW, Penny SG, Ravichandran M (2016) Impact of an upgraded model in the NCEP Global Ocean Data Assimilation System: the tropical Indian Ocean. J Geophys Res Oceans 121(11):8039–8062. https://doi.org/10.1002/2016JC012056

Rahaman H, Venugopal T, Penny SG, Behringer D, Ravichandran M, Raju JVS et al (2018) Improved Ocean analysis for the Indian Ocean. J Oper Oceanogr 12(1):16–33. https://doi.org/10.1080/1755876X.2018.1547261

Rahaman H, Srinivasu U, Panickal S, DurgadooJV GSM, Ravichandran M et al (2020) An assessment ofthe Indian Ocean mean state and seasonal cycle in a suite of interannual CORE-II simulations. Ocean Model 145:101503. https://doi.org/10.1016/j.ocemod.2019.101503

Rao SA, Saha SK, Pokhrel S, Sundar D, Dhakate AR, Mahapatra S, Ali S, Chaudhari HS, Shreeram P, Vasimalla S, Srikanth AS, Suresh RRV (2011) Modulation of SST, SSS over northern Bay of Bengal on ISO time scale. J Geophys Res 116:1–11. https://doi.org/10.1029/2010JC006804

Rao SA, Goswami BN, Sahai AK, Rajagopal EN, Mukhopadhyay P, Rajeevan M et al (2019) Monsoon mission: a targeted activity to Improve Monsoon Prediction across scales. Bull Am Meteorol Soc 100(12):2509–2532. https://doi.org/10.1175/BAMS-D-17-0330.1

Rasmusson EM, Carpenter TH (1982) Variations in tropical sea surface temperature and surface wind fields associated with Southern Oscillation/El Niño. Mon Weather Rev 110(5):354–384. https://doi.org/10.1175/1520-0493(1982)110%3c0354:VITSST%3e2.0.CO;2

Rasmusson EM, Carpenter TH (1983) The relationship between eastern equatorial Pacific sea surface temperature and rainfall over India and Sri Lanka. Mon Weather Rev 111(3):517–528. https://doi.org/10.1175/1520-0493(1983)111%3c0517:TRBEEP%3e2.0.CO;2

Ratna SB, Cherchi A, Osborn TJ, Joshi M, Uppara U (2021) The extreme positive Indian Ocean Dipole of 2019 and Associated Indian Summer Monsoon Rainfall Response. Geophys Res Lett. https://doi.org/10.1029/2020GL091497

Ravichandran M, Behringer D, Sivareddy S, Girishkumar MS, Chacko N, Harikumar R (2013) Evaluation of the global ocean data assimilation system at INCOIS: the tropical Indian Ocean. Ocean Model 69:123–135. https://doi.org/10.1016/j.ocemod.2013.05.003

Reynolds RW, Smith TM, Liu C, Chelton DB, Casey KS, Schlax MG (2007) Daily high-resolution blended analyses for sea surface temperature. J Clim 20(22):5473–5496. https://doi.org/10.1175/2007JCLI1824.1

Ropelewski CF, Halpert MS (1987) Global and regional scale precipitation patterns associated with the El Nino/southern oscillation. Mon Weather Rev 115(8):1606–1626. https://doi.org/10.1175/1520-0493(1987)115%3c1606:GARSPP%3e2.0.CO;2

Ropelewski CF, Halpert MS (1989) Precipitation patterns associated with the high index phase of the southern oscillation. J Clim 2(3):268–284

Rosati A, Miyakoda K, Gudgel R (1997) The Impact of Ocean Initial Conditions on ENSO Forecasting with a Coupled Model. Mon Weather Rev 125(5):754–772. https://doi.org/10.1175/1520-0493(1997)125%3c0754:TIOOIC%3e2.0.CO;2

Saha SK, Pokhrel S, Chaudhari HS, Dhakate A, Shewale S, Sabeerali CT et al (2014) Improved simulation of Indian summer monsoon in latest version of NCEP Climate Forecast System free run. Int J Climatol 34(5):1628–1641. https://doi.org/10.1002/joc.3791

Saha SK, Pokhrel S, Salunke K, Dhakate A, Chaudhari HS, Rahaman H et al (2016) Potential predictability of Indian summer monsoon rainfall in NCEP CFSv2. J Adv Model Earth Syst 8(1):96–120. https://doi.org/10.1002/2015MS000542

Saha SK, Hazra A, Pokhrel S, Chaudhari HS, Sujith K, Rai A et al (2019) Unraveling the mystery of Indian summer monsoon prediction: improved estimate of predictability limit. J Geophys Res Atmos 124(4):1962–1974. https://doi.org/10.1029/2018JD030082

Saranya JS, Roxy MK, Dasgupta P, Anand A (2022) Genesis and trends in marine heatwaves over the tropical Indian Ocean and their interaction with the Indian summer monsoon. J Geophys Res Oceans 127(2):e2021JC017427. https://doi.org/10.1029/2021JC017427

Schlegel RW, Oliver EC, Perkins-Kirkpatrick S, Kruger A, Smit AJ (2017) Predominant atmospheric and oceanic patterns during coastal marine heatwaves. Front Mar Sci 4:323. https://doi.org/10.3389/fmars.2017.00323

Schlegel RW, Darmaraki S, Benthuysen JA, Filbee-Dexter K, Oliver EC (2021) Marine cold-spells. Prog Oceanogr 198:102684. https://doi.org/10.1016/j.pocean.2021.102684

Schott FA, Xie SP, McCreary JP (2009) Indian Ocean circulation and climate variability. Rev Geophys. https://doi.org/10.1029/2007RG000245

Sharma D, Das S, Saha SK, Goswami BN (2022) Mechanism for high "potential skill" of Indian summer monsoon rainfall prediction up to two years in advance. Q J R Meteorol Soc 148(749):3591–3603. https://doi.org/10.1002/qj.4375

Shukla J (1987) Interannual variability of monsoon. In: Fein JS, Stephens PL (eds) Monsoons. Wiley, New York, pp 399–464

Sikka DR (1980) Some aspects of the large-scale fluctuations of summer monsoon rainfall over India in relation to fluctuations in the planetary and regional scale circulation parameters. Proc Indian Acad Sci Earth Planet Sci 89(2):179–195. https://doi.org/10.1007/BF02913749

Simon A, Plecha SM, Russo A, Teles-Machado A, Donat MG, Auger PA, Trigo RM (2022) Hot and cold marine extreme events in the Mediterranean over the period 1982–2021. Front Mar Sci 9:892201. https://doi.org/10.3389/fmars.2022.892201

Stammer D, Köhl A, Awaji T, Balmaseda M, Behringer D, Carton J, Xue Y (2010) Ocean information provided through ensemble ocean syntheses. In: OceanObs 09. European Space Agency, pp 979–989

Storto A, Masina S, Simoncelli S, Iovino D, Cipollone A, Drevillon M et al (2018) The added value of the multi-system spread information for ocean heat content and steric sea level investigations in the CMEMS GREP ensemble reanalysis product. Clim Dyn 53(1):287–312. https://doi.org/10.1007/s00382-018-4585-5

Storto A, Alvera-Azcárate A, Balmaseda MA, Barth A, Chevallier M, Counillon F et al (2019) Ocean reanalyses: recent advances and

unsolved challenges. Front Mar Sci 6:418. https://doi.org/10.3389/fmars.2019.00418
Tang Y, Hsieh W (2002) Hybrid coupled models of the tropical Pacific—II ENSO prediction. Clim Dyn 19(3):343–353. https://doi.org/10.1007/s00382-002-0231-2
Tang Y, Zhang RH, Liu T, Duan W, Yang D, Zheng F et al (2018) Progress in ENSO prediction and predictability study. Natl Sci Rev 5(6):826–839. https://doi.org/10.1093/nsr/nwy105
Taylor KE, Stouffer RJ, Meehl GA (2012) An overview of CMIP5 and the experiment design. Bull Am Meteor Soc 93(4):485–498. https://doi.org/10.1175/BAMS-D-11-00094.1
Thandlam V, Rahaman H, Rutgersson A et al (2023) Quantifying the role of antecedent Southwestern Indian Ocean capacitance on the summer monsoon rainfall variability over homogeneous regions of India. Sci Rep 13:5553. https://doi.org/10.1038/s41598-023-32840-w
Trenberth KE, Branstator GW, Karoly D, Kumar A, Lau NC, Ropelewski C (1998) Progress during TOGA in understanding and modeling global teleconnections associated with tropical sea surface temperatures. J Geophys Res 103(C7):14291–14324. https://doi.org/10.1029/97JC01444
Tsujino H, Shogo U, Nakano H, Small RJ, Kim WM, Yeager SG et al (2018) JRA-55 based surface dataset for driving ocean–sea-ice models (JRA55-do). Ocean Model 130:79–139. https://doi.org/10.1016/j.ocemod.2018.07.002
Venugopal T, Ali MM, Bourassa MA, Zheng Y, Goni GJ, Foltz GR, Rajeevan M (2018) Statistical evidence for the role of southwestern Indian Ocean heat content in the Indian Summer Monsoon Rainfall. Sci Rep 8(1):12092. https://doi.org/10.1038/s41598-018-30552-0
Vialard J, Duvel JP, McPhaden MJ, Bouruet-Aubertot P, Ward B, Key E et al (2009) SupplimenttoCirene: air sea interactions in the Seychelles-Chagos thermocline ridge region. Bull Am Meteorol Soc 90(1):ES1–ES4. https://doi.org/10.1175/2008BAMS2499.1
Wang C, Zhang L, Lee SK, Wu L, Mechoso CR (2014) A global perspective on CMIP5 climate model biases. Nat Clim Chang 4(3):201–205. https://doi.org/10.1038/nclimate2118
Wang C, Zou L, Zhou T (2018) SST biases over the Northwest Pacific and possible causes in CMIP5 models. Sci China Earth Sci 61(6):792–803. https://doi.org/10.1007/s11430-017-9171-8
Wentz FJ, Meissner T, Gentemann C, Hilburn KA, Scott J (2014) Remote Sensing Systems GCOM-W1 AMSR2 [indicate whether you used Daily, 3-Day, Weekly, or Monthly] Environmental Suite on 0.25 deg grid, Version 7.2, [indicate subset if used]. Remote Sensing Systems, Santa Rosa, CA. www.remss.com/missions/AMSR-2. Accessed 25 Mar 2017
Wills RCJ, Dong Y, Proistosecu C, Armour KC, Battisti DS (2022) Systematic climate model biases in the large-scale patterns of recent sea-surface temperature and sea-level pressure change. Geophys Res Lett 49(17):11. https://doi.org/10.1029/2022GL100011
Xie SP, Annamalai H, Schott FA, McCreary JP (2002) Structure and mechanisms of South Indian Ocean climate variability. J Clim 15(8):864–878. https://doi.org/10.1175/1520-0442(2002)015%3c0864:SAMOSI%3e2.0.CO;2
Xue Y, Huang B, Hu ZZ, Kumar A, Wen C, Behringer D, Nadiga S (2011) An assessment of oceanic variability in the NCEP climate forecast system reanalysis. Clim Dyn 37(11):2511–2539. https://doi.org/10.1007/s00382-010-0954-4
Yang Y, Xie SP, Wu L, Kosaka Y, Lau NC, Vecchi GA (2015) Seasonality and predictability of the Indian Ocean dipole mode: ENSO forcing and internal variability. J Clim 28(20):8021–8036. https://doi.org/10.1175/JCLI-D-15-0078.1
Yokoi T, Tozuka T, Yamagata T (2008) Seasonal variation of the Seychelles Dome. J Clim 21(15):3740–3754. https://doi.org/10.1175/2008JCLI1957.1
Yokoi T, Tozuka T, Yamagata T (2009) Seasonal variations of the Seychelles Dome simulated in the CMIP3 models. J Phys Oceanogr 39(2):449–457. https://doi.org/10.1175/2008JPO3914.1
Zebiak SE, Cane MA (1987) A model El Nino-Southern Oscillation. Mon Weather Rev 115(10):2262–2278. https://doi.org/10.1175/1520-0493(1987)115%3c2262:AMENO%3e2.0.CO;2
Zhi H, Zhang R-H, Lin P, Shi S (2019) Effects of salinity variability on recent El Niño events. Atmosphere 10:475. https://doi.org/10.3390/atmos10080475
Zhu J, Kumar A (2019) Role of sea surface salinity feedback in MJO predictability: a study with CFSv2. J Clim 32:5745–5759. https://doi.org/10.1175/JCLI-D-18-0755.1
Zhu J et al (2014) Salinity anomaly as a trigger for ENSO events. Sci Rep 4:6821. https://doi.org/10.1038/srep06821
Zhu J, Huang B, Kumar A, Kinter JL III (2015) Seasonality in prediction skill and predictable pattern of tropical Indian Ocean SST. J Clim 28(20):7962–7984. https://doi.org/10.1175/JCLI-D-15-0067.1
Zuo H, Balmaseda MA, Mogensen K (2015) The ECMWF-MyOcean2 eddy-permitting ocean and sea-ice reanalysis ORAP5. Part 1: implementation. ECMWF Tech Memo 736:1–42
Zuo H, Balmaseda MA, Tietsche S, Mogensen K, Mayer M (2019) The ECMWF operational ensemble reanalysis-analysis system for ocean and sea ice: a description of the system and assessment. Ocean Sci 15(3):779–808. https://doi.org/10.5194/os-15-779-2019